

Copyright Warning & Restrictions

The copyright law of the United States (Title 17, United States Code) governs the making of photocopies or other reproductions of copyrighted material.

Under certain conditions specified in the law, libraries and archives are authorized to furnish a photocopy or other reproduction. One of these specified conditions is that the photocopy or reproduction is not to be “used for any purpose other than private study, scholarship, or research.” If a user makes a request for, or later uses, a photocopy or reproduction for purposes in excess of “fair use” that user may be liable for copyright infringement,

This institution reserves the right to refuse to accept a copying order if, in its judgment, fulfillment of the order would involve violation of copyright law.

Please Note: The author retains the copyright while the New Jersey Institute of Technology reserves the right to distribute this thesis or dissertation

Printing note: If you do not wish to print this page, then select “Pages from: first page # to: last page #” on the print dialog screen

The Van Houten library has removed some of the personal information and all signatures from the approval page and biographical sketches of theses and dissertations in order to protect the identity of NJIT graduates and faculty.

2) **SCHOTTKY-BARRIER SOLAR CELLS;
SURFACE PATTERNING
FOR EFFICIENT LIGHT COLLECTION**

by

) **Constantinos Manolis**

Thesis submitted to the Faculty of the Graduate school
of the New Jersey Institute of Technology in partial
fulfillment of the requirements for the degree of
Master of Science

1989

APPROVAL SHEET

Title of Thesis : Schottky-barrier Solar Cells; Surface
Patterning for Efficient Light Collection

Name and degree : Constantinos Manolis
Master of Science , 1989

Thesis and abstract approved: _____

Dr. Haim Grebel
Associate Professor
Department of Electrical
Engineering

Approval of faculty Committee: _____

Dr. Nuggehalli M. Ravindra
Assistant Professor
Department of Physics

Dr. Marek Sosnowski
Associate Professor
Department of Electrical
Engineering

VITA

Name : Constantinos Manolis

Permanent address: Agios Loukas, Aliveri
Evia-34500, Greece.

Degree and date to be conferred: Master of Science, 1989

COLLEGIATE INSTITUTIONS ATTENDED	DATES	DEGREE	DATE
Bergen Community College, U.S.A.	1981-82		
Montclair State College, U.S.A.	1983-85	BS	1985
New Jersey Inst. of Tech.,U.S.A.	1985-89	MS	1989

Major : Physics, Electrical Engineering

Positions held: Teaching Assistant , from 9/86 to 8/88
Department of Physics
New Jersey Institute of Technology, U.S.A.

Title of Thesis: Schottky-barrier Solar Cells; Surface Patterning for Efficient Light Collection.

Constantinos Manolis, Master of Science, 1989

Thesis directed by: Dr. H. Grebel, Associate Professor of Electrical Engineering Department.

ABSTRACT

Different geometrical surface configurations are considered here for a Au/n-Si semiconductor Schottky-barrier solar cell to improve their light collection efficiency.

Optical and electrical properties are theoretically analyzed for two given optical wavelengths of 0.9 and 0.5 micrometers respectively.

The configurations considered are: V-shaped, Star-shaped, M-shaped, asymmetric-V-shaped, and asymmetric-M-shaped. They all show a significant improvement in the short-circuit current over a flat cell model, while the open-circuit voltage remains practically unchanged.

Blank Page

CONTENTS

I	INTRODUCTION	1
II	ANALYSIS OF THE DIFFERENT SURFACE CONFIGURATIONS.....	13
	2.1 Background	13
	2.2 Reflectivity of cell surface.....	20
	2.3 The Multiplicity Factor - An Electrical Property....	26
	2.4 The Surface Configurations - Calculations.....	36
	(a) Flat - surface cells.....	36
	(b) V-shaped surface cells.....	37
	(c) Star-shaped surface cells and the Inverted - -star cells.....	45
	(d) M-shaped surface cells.....	51
	(e) Asymmetric V-shaped surface cells.....	57
	(f) Asymmetric M-shaped surface cells.....	64
	2.5 Noise Corrections.....	66
III	DISCUSSION.....	76
IV	CONCLUSION.....	79
	Appendix A - Numerical Solution Method/Computer Programs....	80
	Appendix B - Photogenerated Current/ Computer Program.....	90
	BIBLIOGRAPHY	94

List of Symbols

Symbol	Description
A	Total diode (top) surface area
A**	Effective Richardson constant
C	Speed of light in vacuum
d	Thickness of the metal film
dY	Curved length of the field (electric) line
D _{n,p}	Electron, hole diffusion constants
E _g	Bandgap energy
E _{ph}	Photon energy
F(λ)	Number of incident photons (per cm ² sec)
G	Generation rate of carriers
h	Horizontal length (along x-axis)
I	Current
I _s	Saturation current
I _{sc}	Short-circuit current
J _b	Bulk photocurrent density
J _d	Depletion region photocurrent density
J _L	Total photocurrent density
J _m	Metallic film photocurrent density
k	Extinction coefficient
K	Boltzmann's constant
L	Perpendicular distance from the top to the flat back surface

$L_{n,p}$	Diffusion length of electrons, holes
m	Number of (flat top section) sides in a unit cell
n_i	Complex index of refraction
n_p	Excess electron concentration in p-type
n_s	Substrate index of refraction (real)
N	Number of discrete area sections
p_n	Excess hole concentration in n-type
q	Electron charge
r	Arc radius
$r_{,r}$	Parallel, perpendicular reflection coefficients
$R(\lambda)$	Reflectivity
S	Total length of one side (top sections)
T	Temperature
$T(\lambda)$	Transmission coefficient
V	Voltage
V_{bi}	Built-in-potential
V_{oc}	Open-circuit voltage
W	Depletion region width
x	Distance, depth in the bulk
x_0	Light path distance entering the top surface
Y	Constant linear length of field line (=50 μm)
Y_0	Linear length path of field (electric) line
Y_T	Total length of the field (electric) line

α Absorption coefficient

γ	Insulating thickness
δ	Penetration depth or skin depth
ΔA	Unit area of each section
ϵ	Electric field
η	Ideality factor
θ	Angle of incidence
θ_0	Angle facing the arc (curvature of field line)
λ	Wavelength
$\mu_{n,p}$	Electron, hole mobility
ξ	Multiplicity factor
$\tau_{n,p}$	Electron, hole lifetimes or decay times
φ	Angle of refraction
Φ_B	Barrier height between metal-semiconductor
Φ_T	Average barrier height by insulating layer
Ψ	Amplitude of pattern (=50 μm)
ω	Angular frequency
ω_p	Plasma frequency

I Introduction

Solar cells have provided electrical power source for space vehicles, consumer calculators, and watches. In the last decade or so it approaches the stage at which solar power plants can be built giving million of watts of power worldwide. A solar cell is a device (primarily a semiconductor) that converts solar radiation (solar photons) into electrical power. When those solar photons, of about 0.1 watts per square centimeter power at air mass one (AM 1) strike a semiconductor on the surface of the earth, they may be reflected, transmitted, or absorbed. The photons that are absorbed by the solar cell are the ones of potential use .

An energetic photon that is absorbed in a semiconductor may remove an electron from the valence band to the conduction band or produce heat through lattice vibrations. We note that there is a band gap E_g between the bottom of the conduction band and the top of the valence band. When an electron makes a transition from the valence band to the conduction band and requires only an energy change ($\geq E_g$), then the semiconductor is said to have a direct intrinsic band gap, shown in Fig. (A-(1)). Both GaAs and Cds have direct band gaps. On the other hand when this transition requires not only an energy change ($\geq E_g$) but also some change in the crystal momentum for the electron, then the semiconductor is

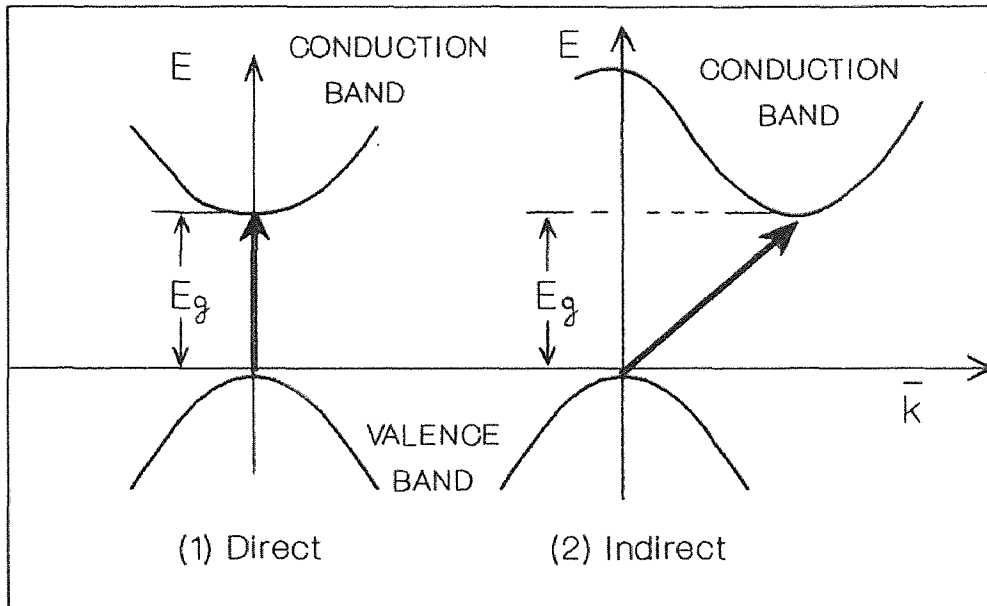


Fig.(A) Electron transitions in semiconductors; Ref.[2].

said to have an indirect intrinsic band gap, shown in Fig.(A-(2)), [1],[2]. Both Ge and Si are indirect gap materials. For example, in the indirect gap Si semiconductor, a photon with wavelength shorter than 1.1 μm has enough energy to produce a free electron when it is absorbed. The band gap energy (E_g) for silicon is about 1.1 eV and the corresponding wavelength is: $\lambda(\mu\text{m}) = 1.24/E_g$ (eV). Due to indirect transition in silicon some of the photonic energy will result in lattice vibrations or heat.

When light is absorbed in a semiconductor it produces two types of free carriers: the free electron in the conduction band and the free hole in the valence band. Carriers will be generated and current will be produced continuously, for as long as the cell is exposed to light. We have to keep in mind here that whatever conductor (metal, or semiconductor) we place on the top (front surface) of the light-absorbing semiconductor it has to be transparent enough in order for sunlight to pass through it and be absorbed. Two critical factors, the band gap and the absorption coefficient, determine the absorption of light along with the thickness of the cell. The band gap (mentioned above) is the characteristic energy level above which the cell begins to absorb sunlight. Materials which have low bandgaps are preferred (Si with 1.12 eV, GaAs with 1.424 eV), to take advantage of larger fraction of the available sunlight. It is observed that different semiconductor

materials absorb sunlight best at different thicknesses, which can range from about a reasonable 100 μm or more to lately reported even less than 1 μm (thin-film solar cells), [3],[4],[5].

Several other phenomena are of interest in understanding the performance of a well-designed solar cell. When an n-type semiconductor and a p-type semiconductor are put together in such a way that their fermi levels line up to form a junction, then, a band bending occurs creating a difference between the p-side and the n-side neutral regions which is called the built-in potential V_{bi} , shown in Fig.(B). This transition region, where the bands bent, is called the depletion region and the densities of the mobile carriers are equal to zero. Carriers generated, from incident photons, under the influence of an electric field (due to the built-in potential), produce a so called, drift current. Due to this process, these carriers will be accelerated along the electric field, within the depletion region in opposite directions to each other, as shown in Fig.(B). If there is a spatial variation of carrier concentration in the semiconductor then the carries tend to move from a region of high concentration to a region of low concentration creating the so called, diffusion current, shown in Fig.(B). At thermal equilibrium, that is, the steady-state condition, (without external excitations) at given temperature, the net current flow across the junction is zero.

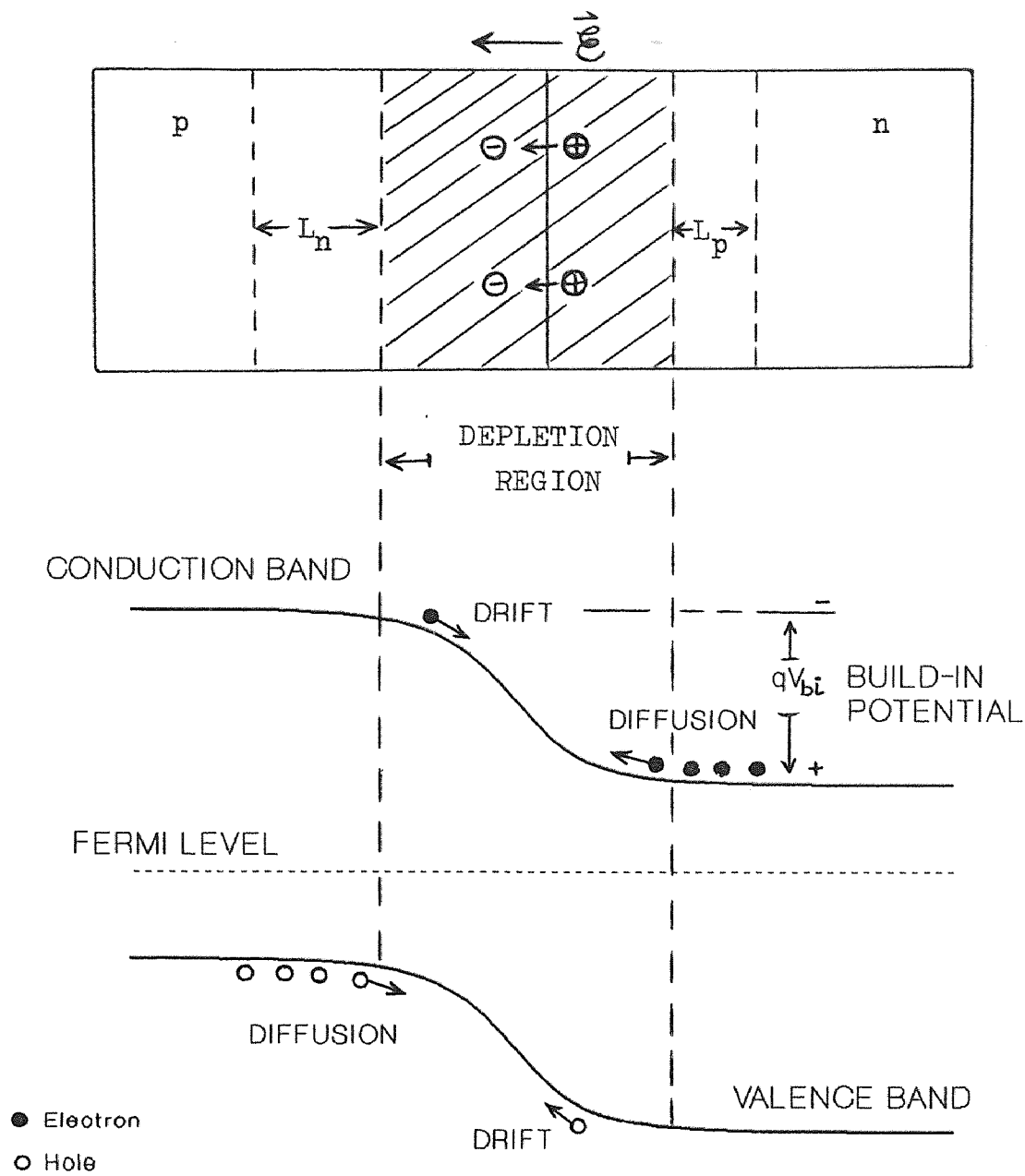


Fig.(B) A p-n junction in thermal equilibrium; Ref.[1].

Thus, for each type of carrier, the drift current due to electric field must exactly cancel the diffusion current due to the concentration gradient, [1].

Many of the useful properties of a p-n junction can be achieved by simply forming an appropriate metal/semiconductor contact. A metal - semiconductor or Schottky barrier junction will be our model solar cell in this work and it is chosen because of low-cost, low-temperature, and ease of fabrication technology. Usually on a Schottky-barrier solar cell a junction is produced when a low work function metal (like Al) is deposited onto a p-type semiconductor or a high work function metal (like Au) is deposited onto a n-type semiconductor. This barrier contact is in contrast to the low-resistance ohmic contact usually required for metallic contacts to semiconductor devices. This barrier creation is important to the flow of majority carriers from the semiconductor to the metal. The current transport in metal-semiconductor contacts is due mainly to majority carriers, in contrast to p-n junctions, where current transport is due mainly to minority carriers. The band bending in the semiconductor produces a built-in potential that determines the open-circuit voltage (V_{oc}) in the solar cell, (Fig.(C)). This built-in potential is simply the difference in work function between the metal and the semiconductor while the barrier height is the energy difference between the work

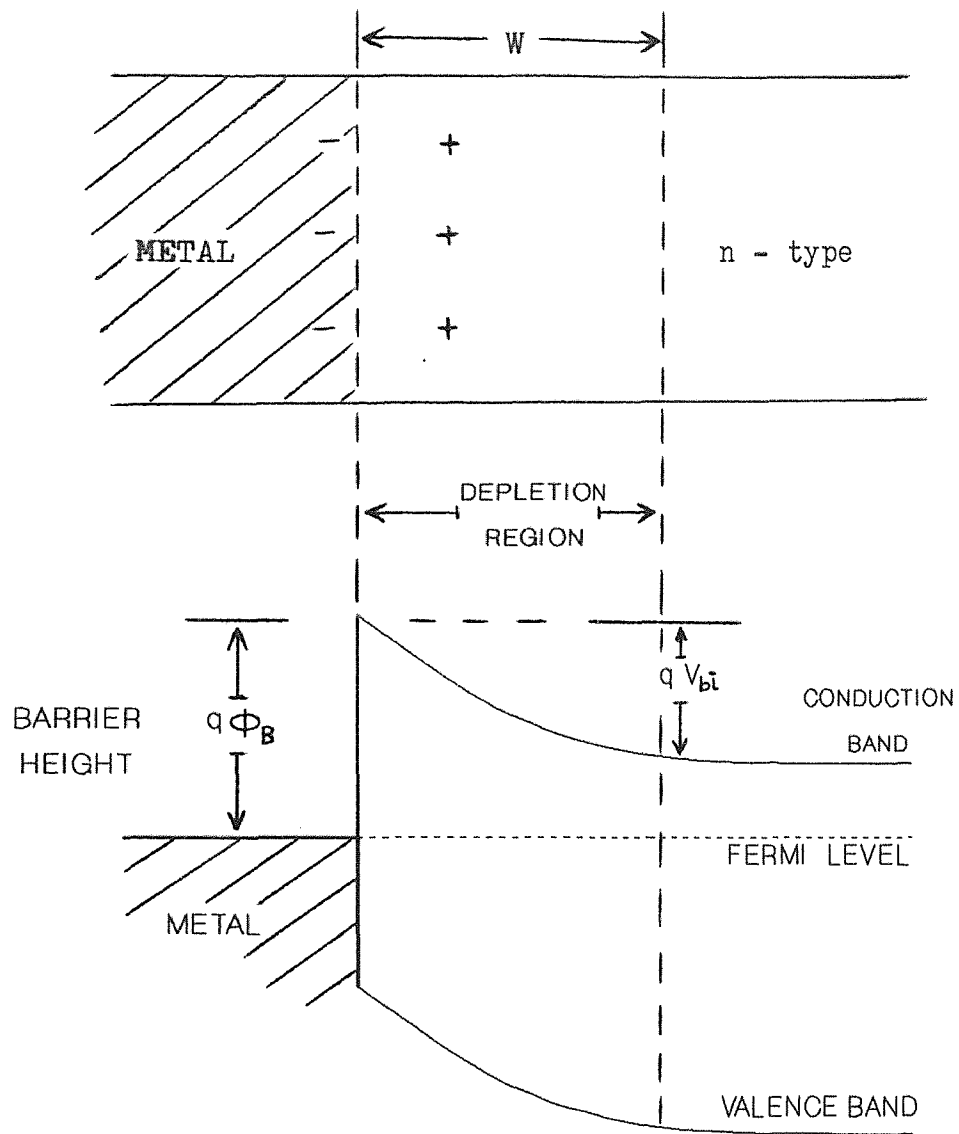


Fig.(C) The equilibrium band diagram of a Schottky barrier of n-type semiconductor; Ref.[2]

function of the metal and the top of the valence band (for p-type semiconductors) or the bottom of the conduction band (for n-type). The electric field and the bending of the bands within the depletion region ($-W$) are similar to effects already discussed for p-n junction, [2],[3].

In our work the metal is a thin film of Au (gold) in the order of about 90 - 100 \AA as minimum metallic thickness, to optimize for the optical as well as the electrical properties, and the semiconductor will be a n-type silicon.

Of course, not everything works perfectly, ideally. Heat, light reflection, photons that are not absorbed by the semiconductor, series resistance, carrier recombination, are some of the major factors, losses that someone should account and be aware of when studying solar cells. In order to improve one of the above mentioned factors that contribute to loss, the reflection of the incident light, we present different geometrical surface configurations, "texturizing" surface, to increase the number of reflections and therefore the photocurrent generated, before light escapes back to space. Since most semiconductor materials have a high reflectivity (in our case 31-34 % for perpendicular incidence on Si) it will be shown with our work that, in some cases and portions of the surface area we got less than 10 % of the light reflected back. These results and calculations are done without any antireflection coating on the textured surfaces,

application of which may decrease reflection losses even further. Calculations are done for two different wavelengths: $0.9 \mu\text{m}$, where the spectral irradiance (at AM 1) is rather small and the energy of photons close to the band gap energy for Si; and at $0.5 \mu\text{m}$ where spectral irradiance reaches its maximum value and the energy of photons much higher (doubled) than the band gap energy of Si. We do understand at this point that photons at $0.5 \mu\text{m}$ wavelength, if absorbed by the semiconductor will give about half of their photonic energy as heat dissipation in the material through lattice vibrations, resulting in a decrease of the cell efficiency. Although this heat dissipation is expected, we do believe that it does not affect our calculations, since it will be equally effecting all of our configurations discussed. After all, this kind of solar irradiance is there and cannot be ignored.

Researchers in the past around mid-70's have spent time with the formation of randomly distributed regular pyramids on the surface of a Si semiconductor for space applications which proved as reported to a significant reduction in the overall reflectance over the flat polished silicon cell surface [6],[7]. Their reflectance was reaching zero values with the addition of tantalum oxide as an anti-reflection coating over a wavelength range from $0.5 \mu\text{m}$ to almost $1.0 \mu\text{m}$. Also it was claimed that because of this surface texture a reduction in cell length would be advised because 84 % of all

carriers produced was within the first 45 μm whereas only 26 % was with a flat polished surface cell, within the same distance. This type of cell was providing higher short-circuit current due to a reduction in the reflectance of incident light.

The V-grooved silicon solar cells reported also in the mid-70's showed an improvement in the reflection of light from 30% for a flat cell to about 9 % for a grooved surface [8]. This reflection reduction was essentially independent of the wavelength of the incident light. The absorption and carrier generation occurred closer to the junction and collection efficiency was improved. It was also taking into account some internal total reflection on a rear smooth surface, which improved further the total efficiency. It was observed that current collected at the peaks of the grooved surface was about 80 % to that collected in the valleys.

Efficiencies were at about 12 % which indicated that texturized or grooved surfaces do not "adversely" effect the cell.

In more recent research in 1987 a substrate with a pyramidally textured top surface and a planar reflecting bottom surface (Lambertian scheme) was very successful because of its use in point contact solar cells where they proved to demonstrate efficiencies of 27.5 % under concentrated sunlight [9]. Pyramidal texturing of the surface of a substrate could

give rise to a significant degree of light trapping within the substrate. This effect could maximize the efficiency of silicon photovoltaic devices where pyramidal texturing was commonly used for reflection control.

The V-Grooved multijunction solar cell, should have a conversion efficiency greater than 20 % because of its high collection efficiency (95 % of incident photons absorbed), lower series resistance, and no shadowing effect on the illuminated surface because it has no collection grids [10]. This cell has a trapezoidal shape and consists of many individual p^+n-n^+ / p^+p-n^+ diode elements connected in series.

The tandem-junction solar cell combines the back-surface-field cell and the textured cell [11]. It uses thinner base material and it behaves like a bipolar transistor with expected efficiency of more than 20 %.

It would be a great omission if we do not mention about today's research in the solar cell technology in this direction, in using the incident light more efficiently. Nowadays, scientists and engineers work over the so called stacked cells which consist of two or more photovoltaic, semiconductor materials one on the top of the other to absorb the light spectrum more efficiently than a single material alone. Just recently Sandia National Laboratories announced that a GaAs cell (which absorbs more of the visible light) on top of a crystalline Si (which uses the transmitted infrared

light) reaches efficiency of 31 % [12].

In the following, we consider a textured solar cell to improve light collection efficiency with minimal degradation of the electrical properties of the cell. We have chosen a Schottky type solar cell since it offers ease of fabrication, though with the penalty of reduced efficiency. To overcome this deficiency we suggest to coat the whole front face of the cell with a conductor, in contrast to 50 % metalization of today's cells. All in all, we believe that the reduced costs with an increase in efficiency will make this cell more applicable for commercial uses.

II ANALYSIS OF THE DIFFERENT SURFACE CONFIGURATIONS

2.1 Background

A Schottky-barrier solar cell, consists of a metal (thin, mostly transparent and here gold) at the surface followed by a semiconductor (here a n-type single crystal Si also referred to as the base and an ohmic (of negligible resistance) back contact.

This solar cell under illumination will have three photocurrent components that contribute to the total photogenerated current, given by:

$$J_L = J_m + J_d + J_b \quad (1)$$

where: J_L --is the total photocurrent density (A/cm^2)

J_m --is the metallic film photocurrent density due to absorption in the metal (A/cm^2),

J_d --is the depletion region photocurrent density (A/cm^2),

and J_b --is the bulk (base) region photocurrent density (A/cm^2).

Short-wavelengths (UV, near visible regions) are mostly absorbed in the depletion region, whereas, long-wavelengths (Near IR) are mostly absorbed in the, bulk region. Light that has energy larger than that indicated by the barrier

height ($q\Phi_B$) can be absorbed in the metal and, therefore, excite carriers into the semiconductor. It was found [13] that this type of current contributes very little (less than 1 %) to the total photocurrent and, therefore, J_m will be neglected from our calculations. We are left with the two major contributors to the photocurrent, J_a and J_b . So:

$$J_L(\lambda) = J_a(\lambda) + J_b(\lambda) \quad (1.1)$$

Because of the high electric field in the depletion region, the photogenerated carriers will be swept out before they recombine creating a photocurrent given by [3]:

$$J_a = q T(\lambda) F(\lambda) [1 - \exp(-\alpha W)] \quad (2)$$

where: q --is the electron charge (1.6×10^{-19} cb),

$T(\lambda)$ --is the transmission coefficient at the metal/semiconductor interface (for a single λ),

$F(\lambda)$ --is the number of incident photons per cm^2 per sec per unit bandwidth (flux),

α -- is the absorption coefficient (cm^{-1}),

and W -- is the depletion region width (cm).

The transmission coefficient has a dependency on the angle of incidence (θ), $T(\lambda, \theta)$, which is discussed in more details in the next section. The absorption coefficient also has a

dependency on the angle of refraction (φ) according to [7]:

$$\alpha(\lambda, \varphi) = \alpha(\lambda) / \cos \varphi \quad (3)$$

It was found, that, $\alpha(\lambda) = 500 \text{ cm}^{-1}$ at $\lambda = 0.9 \text{ }\mu\text{m}$, and $\alpha(\lambda) = 10000 \text{ cm}^{-1}$ at $\lambda = 0.5 \text{ }\mu\text{m}$ [1]. Non-perpendicular light incidence travels a depletion region given by:

$$W(\varphi) = W / \cos \varphi \quad (4)$$

where a typical value of $2.5 \text{ }\mu\text{m}$ was used for the W [13]. The number of incident photons was calculated by using the solar spectral irradiance data at AM1, [1],[14]. At $\lambda=0.9 \text{ }\mu\text{m}$ over a bandwidth of $\Delta\lambda= 0.04 \text{ }\mu\text{m}$, and with an average energy per photon of, $E_{ph} = 1.24 / 0.9 \text{ }\mu\text{m} = 1.4 \text{ eV}$ the number of photons will be:

$$F(\lambda) = 1.4 \times 10^{18} \text{ photons/cm}^2 \text{ sec} \quad (5)$$

At $\lambda = 0.5 \text{ }\mu\text{m}$ the number of photons is:

$$F(\lambda) = 1.8 \times 10^{18} \text{ photons / cm}^2 \text{ sec} \quad (6)$$

It is worth noting here, that the total number of solar photons at sea level is about $4.8 \times 10^{17} \text{ cm}^{-2} \text{ sec}^{-1}$ and the

maximum number of them to be absorbed in Si is about $3.7 \times 10^{17} \text{ cm}^{-2} \text{ sec}^{-1}$ (or 77 %) [15].

When light of a given wavelength λ is incident on the front surface, the photocurrent can be derived. If we assume that each incident photon, at each wavelength, generates a pair of carriers, then the generation rate of electron-hole pair at some distance x_0 from the semiconductor surface will be given by [3]:

$$G(\lambda, x) = \alpha(\lambda) F(\lambda) [1 - R(\lambda)] \exp[-\alpha(\lambda) x_0] \quad (7)$$

where: $R(\lambda)$ -- is the fraction of photons reflected from the surface (reflectivity),

and $T(\lambda) = 1 - R(\lambda)$.

The one-dimensional steady-state continuity equations are [3]:

-for electrons in p-type-

$$G_n - (n_p/\tau_n) + (1/q)(dJ_n/dx) = 0 \quad (8)$$

-for holes in n-type-

$$G_p - (p_n/\tau_p) - (1/q)(dJ_p/dx) = 0 \quad (9)$$

where: n_p, p_n -- are the excess electron, hole concentrations in p-type and n-type respectively,

τ_n, τ_p -- are the electron and the hole lifetimes (sec)
 J_n, J_p -- are the current-densities (A/cm²),
 x_0 -- is the light path from the top surface,
 x -- is the distance, -depth in the bulk and for
our case is actually taking values from:
 $x = (Y_0 + Y) + dY$ (the linear $(Y_0 + Y)$ - and the
non-linear, curved portion dY - of the field
line) as it will be discussed later in
section 2.3.

The current density equations are given by:

$$J_n = q \mu_n n_p \epsilon + q D_n (dn_p/dx) \quad (10)$$

$$J_p = q \mu_p p_n \epsilon - q D_p (dp_n/dx) \quad (11)$$

where: $q \mu_n n_p \epsilon ; q \mu_p p_n \epsilon$ -- are the Drift components,
 $q D_n (dn_p/dx) ; q D_p (dp_n/dx)$ -- are the Diffusion
components,
 ϵ -- is the electric field,
 D_n, D_p -- are the electron and hole diffusion constants
respectively (cm²/sec).

For an n-type semiconductor equations (7), (9), and (11) can
be combined to yield the following differential continuity
equation [3]:

$$D_p \frac{d^2 P_n}{d x^2} - \frac{P_n}{\tau_p} + \alpha(\lambda) F(\lambda) T(\lambda) \exp(-\alpha(\lambda)x) = 0 \quad (12)$$

A general solution to the above differential equation (12) with the boundary conditions $p_n = 0$ at: $x = W$ and $x = L$, results in the hole photocurrent density collected at the depletion edge, $x = W$, given by [13]:

$$J_b(\lambda) = \frac{q \alpha(\lambda) F(\lambda) T(\lambda) L_p}{(\alpha^2 L_p^2 - 1)} \{ (\alpha L_p - 1) \exp(-\alpha W) + \frac{2[\exp(-\alpha L) - \exp(-\alpha W)(\exp(W-L/L_p))]}{(\exp(L-W/L_p) - \exp(W-L/L_p))} \} \quad (13)$$

where the new parameter in here L_p is the hole-diffusion length and its value is given by:

$$L_p = (D_p \tau_p)^{1/2} \quad (14)$$

A typical value for Si at 300° K used in our calculations is - for $D_p = 12.5 \text{ cm}^2/\text{sec}$ [2] and $\tau_p = 0.3 \text{ } \mu\text{sec}$ [1] - $L_p = 20 \mu\text{m}$. Now collecting some of our values at this point for a cell of total (maximum) length $L = 100 \mu\text{m}$ with $W = 2.5 \mu\text{m}$ and $L_p = 20 \mu\text{m}$ one can very easily find out that the last term inside the brackets in equation (13) is almost zero and can be neglected.

$$\frac{2[\exp(-\alpha L) - \exp(-\alpha W)(\exp(W-L/L_p))]}{(\exp(L-W/L_p) - \exp(W-L/L_p))} = 0 \quad (15)$$

Therefore equation (13) becomes:

$$J_b(\lambda) = \frac{q \alpha(\lambda) F(\lambda) T(\lambda) L_p}{(\alpha^2 L_p^2 - 1)} \{(\alpha L_p - 1) \exp(-\alpha W)\} \quad (16)$$

and by doing a simple algebraic calculation in equation (16) we get:

$$J_b(\lambda) = \frac{q \alpha(\lambda) F(\lambda) T(\lambda) L_p}{(\alpha L_p + 1)(\alpha L_p - 1)} \{(\alpha L_p - 1) \exp(-\alpha W)\} \Rightarrow$$

$$J_b(\lambda) = \frac{q \alpha(\lambda) F(\lambda) T(\lambda) L_p}{(\alpha L_p + 1)} [\exp(-\alpha W)] \quad (17)$$

Now equation (17) is the final form of our bulk component of the photocurrent which along with equation (2) give us the total photogenerated current density for a Schottky barrier solar cell.

Once the total photogenerated current is calculated, one can find the I-V characteristic of the Schottky barrier cell under illumination. For this, first, it will be necessary to calculate the saturation current I_s which is given by [16]:

$$I_s = A A^{**} T^2 \exp(-q\Phi_{Bn}/KT) \quad (18)$$

where: A--is the total diode area (cm²)

A^{**} -- is the effective Richardson constant (for n-type Si is $110 \text{ A/cm}^2/\text{K}^2$)

T -- is the temperature (300° K)

$q\Phi_{Bn}$ -- is the barrier height between metal-semiconductor taken here to be equal to $2/3 E_g = 1.2 \times 10^{-19} \text{ J}$

K -- is the Boltzmann's constant ($1.38 \times 10^{-23} \text{ J/K}$)

Now the I-V characteristic equation will be given by [3]:

$$I = I_L + I_s (1 - \exp(qV/\eta KT)) \quad (19)$$

The parameter n in the above equation represents an ideality factor which will be taken to be equal to one ($\eta = 1$) for our calculations.

2.2 Reflectivity of cell surface

In general, the reflectivity (R) of most metals depends more on the wavelength than on the angle of incidence and it is usually high. But as discussed in the introduction, for our Schottky barrier we need an almost transparent medium on the front surface to assure that enough light, if not all, gets into the semiconductor substrate. This can be achieved if the thickness of the metal on the surface is substantially small (thin-film), though not as small as to lose the electrical properties of the metal. It was found that, for a thickness

of 100^oA of Au on a n-type Si over a range of λ between 0.5 μm - 1.1 μm that the absorption of light in the metal is almost zero (see fig.1), [13].

Also, the transmittance (T) for a film bounded by air (index of refraction 1.0) and a substrate of refractive index n_s , on which the film is deposited, is given to a first approximation by, [17]:

$$4 n_s / T = (\omega_p / \omega)^2 \sinh^2(d/\delta) \quad \text{or}$$

$$T(\lambda) = (\omega / \omega_p)^2 (4 n_s / \sinh^2(d/\delta)) \quad (20)$$

where: ω_p -- is the plasma frequency

δ -- is the penetration depth or skin depth and for Au is about 210 ^oA ; $\delta = C / \omega_p$,

d -- is the thickness of the metal film (^oA)

and, $\omega = 2\pi \nu = 2\pi C / \lambda$.

Now from $\omega_p = C / \delta$ we get:

$$\omega_p = 1.5 \times 10^{16} \text{ (rad/sec)}.$$

Since the transmission is optical wavelength dependent, a minimum metallic thickness value of about, $d = 90 - 100$ ^oA will be used to optimize for the optical as well as the electrical properties. For both wavelengths of 0.9 and 0.5 μm the metallic film is transparent, shown by equation (20), and all light is transmitted through the metal for the above given

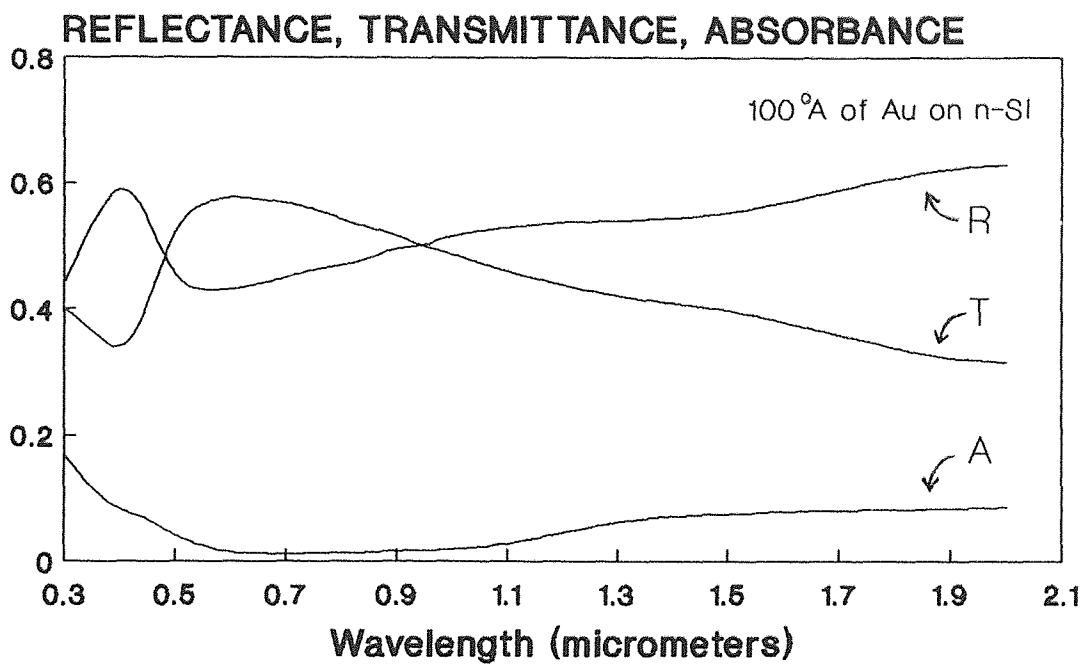


Fig.(1) Optical characteristics of the gold/n-silicon system.
 (R.F.McOuatt and D.L.Pulfrey; Ref.[13])

wavelengths and thickness.

The index of refraction of an absorbing medium is complex and given by:

$$n_1 = n_s - ik \quad (21)$$

where: k -- is a parameter called the extinction coefficient,

$$\text{with } k = \alpha \lambda / 4 \pi.$$

By checking some values of n_s and k for Si at different wavelengths [18] we find that: at $0.3\mu\text{m}$ - where Si is strongly absorbing - $n_s = 5.0$ while $k = 4.2$; at $0.5 \mu\text{m}$ $n_s = 4.3$ and $k = 0.073$; at $0.9 \mu\text{m}$ $n_s = 3.5$ and $k = 7.0 \times 10^{-3}$; so k becomes significantly small, and is neglected.

The reflectance (R) is given by [19]:

$$R = |r_{\parallel}|^2 = |r_{\perp}|^2 = \frac{(n_s - 1)^2 + k^2}{(n_s + 1)^2 + k^2} \quad (22)$$

where: r_{\parallel} and r_{\perp} -- are the parallel and the perpendicular amplitude reflection coefficients of the Fresnel's equations.

Neglecting the k^2 term at $\lambda = 0.9$ and $0.5 \mu\text{m}$, we get:

$$R(\lambda) = \frac{(n_s - 1)^2}{(n_s + 1)^2} \quad (23)$$

Now when the light is not perpendicularly incident the reflectivity (R) will be increasing as the angle of incidence (θ) increases reaching a value of $R = 1$ at $\theta = 90^\circ$. For this case we approximate that the value for the reflectivity to be given by the most dominant perpendicular reflection coefficient r_{\perp} . Assuming also here that the thin film of Au remains to a great extent transparent in this case we can get the value of reflectivity, [19]:

$$R(\lambda, \theta) = |r_{\perp}|^2 = |(E_r/E_i)|^2 = \frac{\sin^2(\theta - \varphi)}{\sin^2(\theta + \varphi)} \quad (24)$$

where: φ -- is the refracted angle calculated by Snell's law:

$$\varphi(\lambda, \theta) = \arcsin(\sin\theta / n_s) \quad (25)$$

How reflectivity varies with angle of incidence is shown in fig.(2). The transmissivity (T) will be given by:

$$T(\lambda, \theta) = 1 - R(\lambda, \theta) \quad (26)$$

When light impinges on a grooved surface it may experience more than one reflections. Each time the light hit the surface, a lesser and lesser amount of photons will be reflected and, therefore, transmitted into the semiconductor to be absorbed.

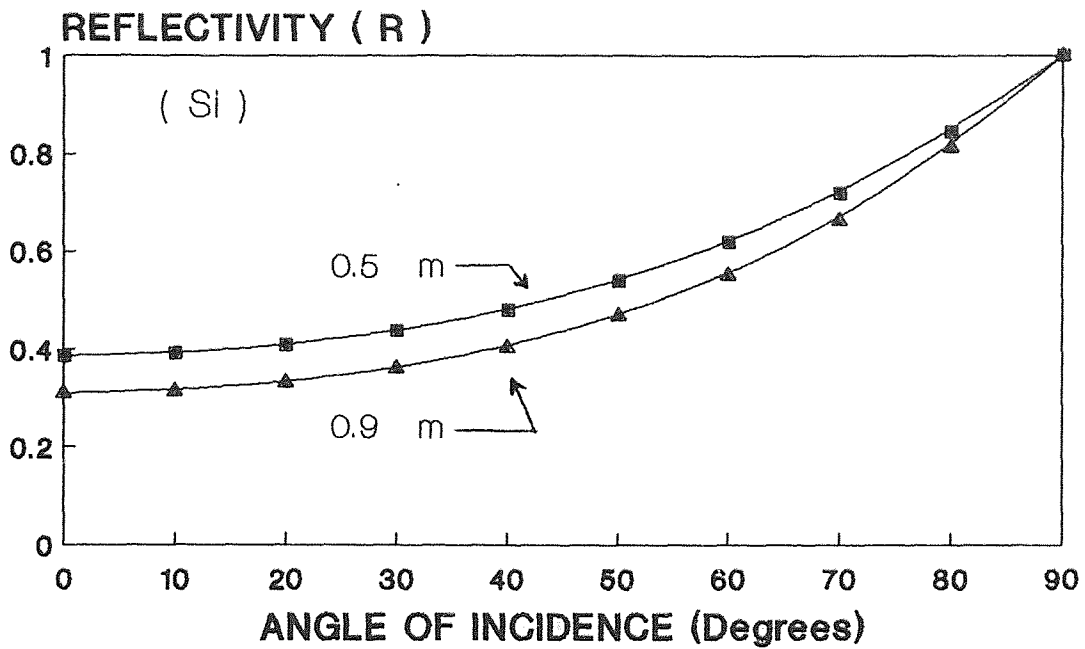


Fig.(2) Reflectivity Vs. angle of incidence on a Si surface at 0.9 and 0.5 micrometer wavelengths.

Finally, almost all photons are transmitted through the metal. Define θ_1 , R_1 , F_1 as the incident angle, the reflectivity, and the total number of incident photons respectively for the first reflection, and θ_2 , R_2 , F_2 for the second reflection. Then, the number of photons incident at the second time will be:

$$F_2 = R_1 F_1 \quad (27)$$

and the number of those transmitted during the second time will be:

$$T_2 (R_1 F_1) \quad \text{or} \quad (1 - R_2) R_1 F_1 \quad (28)$$

For the third reflection: $T_3 (R_2 R_1 F_1)$, and so on.

The total photocurrent, $J(\lambda)$ depends on the incident photon flux through Eqs. (1.1), (2), and (17).

We should note, though, that some of the transmitted light is transformed into heat (particularly photons with energies much higher than the band-gap energy of the semiconductor) and, therefore, is considered as loss. Nevertheless, our aim is to maximize the light transmission through solar cell surface patterning.

2.3 The Multiplicity Factor - An Electrical Property

Homogeneous flat front/back surface solar cells possess

equipotential lines which are straight and parallel to the surfaces. The electric field lines are perpendicular at each point to those equipotential lines. Non-flat front surface solar cells exhibit non-flat equipotential surface and non-uniform electric field lines. Equipotentials, for some configurations used in our work, are shown in Figs.(3) to (6). A numerical method is used to create these lines, [20], (see appendix A for potential points generation, through use of computer programs). We comment that solving Laplace's equation is justified since most of carriers generated, for $\lambda = 0.5 \mu\text{m}$, occur in the depletion region. The depletion region is very small compared to the bulk dimensions of the solar cell. For $\lambda = 0.9 \mu\text{m}$, the Poisson's equation should be solved for the equipotential lines. Nevertheless we assume that the major field distribution will be due to the static Laplace problem. The curved field lines will modify our computation of L , the effective cell thickness, needed for the photogenerated current J_L . We divide the field line into a straight part (Y_0+Y) , and a curved part dY . The curved part is approximated by an arc with a radius of r_j . This radius r_j takes values from 0 to S (the total length of one side at the highest point). This is illustrated in Fig.(7). Therefore $dY_j = r_j \theta_0$ gives us the length of this curved part for different r_j values, (for example, θ (of the V grooves) = 50° , with curvature angle to be equal to 10°). The total length Y_T of

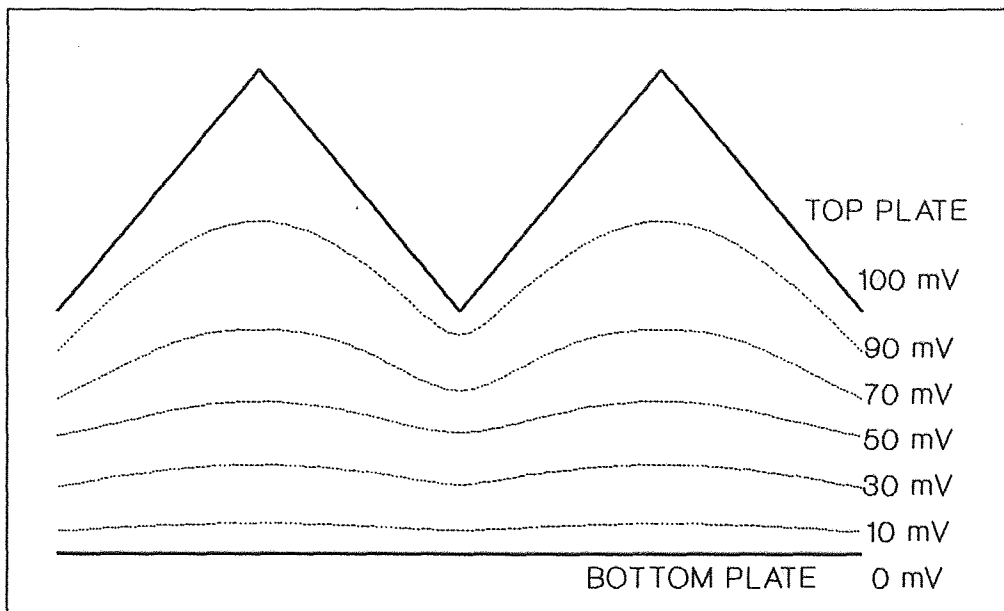


Fig.(3) Equipotential lines for the V-shaped surface cell.

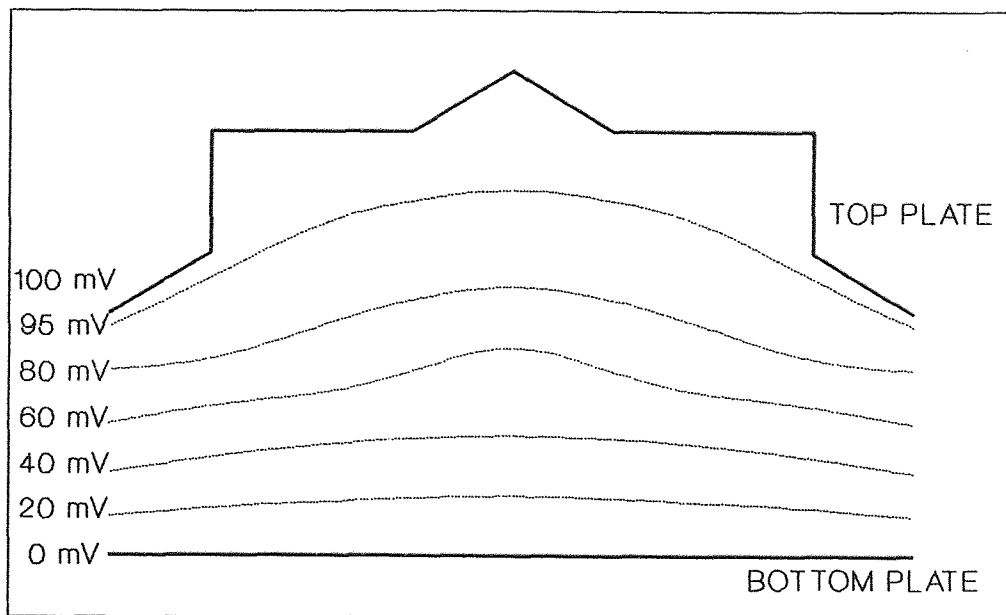


Fig.(4) Equipotential lines for the Star-shaped surface cell.

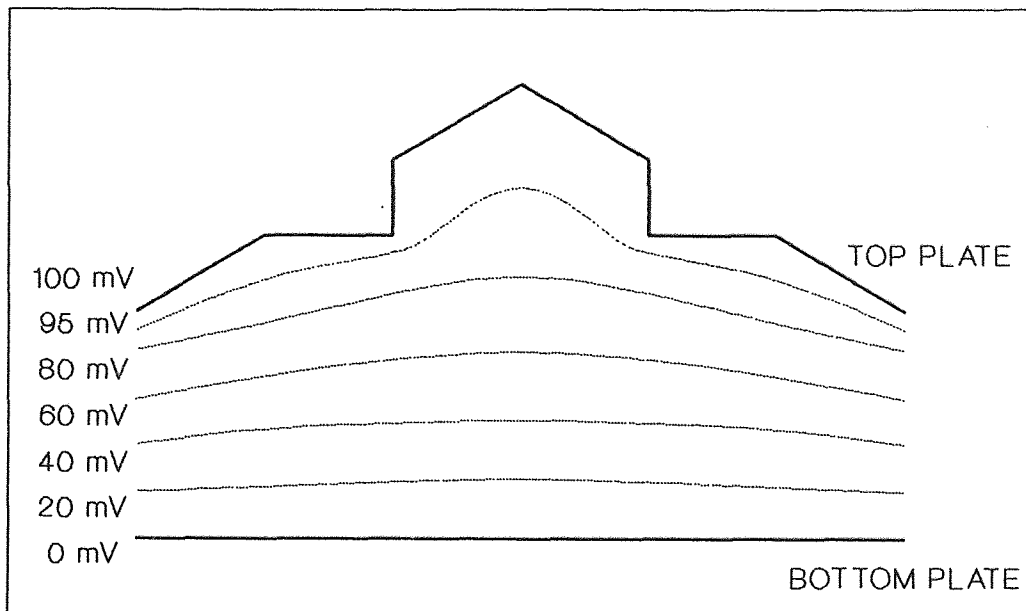


Fig.(5) Equipotential lines for the inverted-star-shaped surface cell.

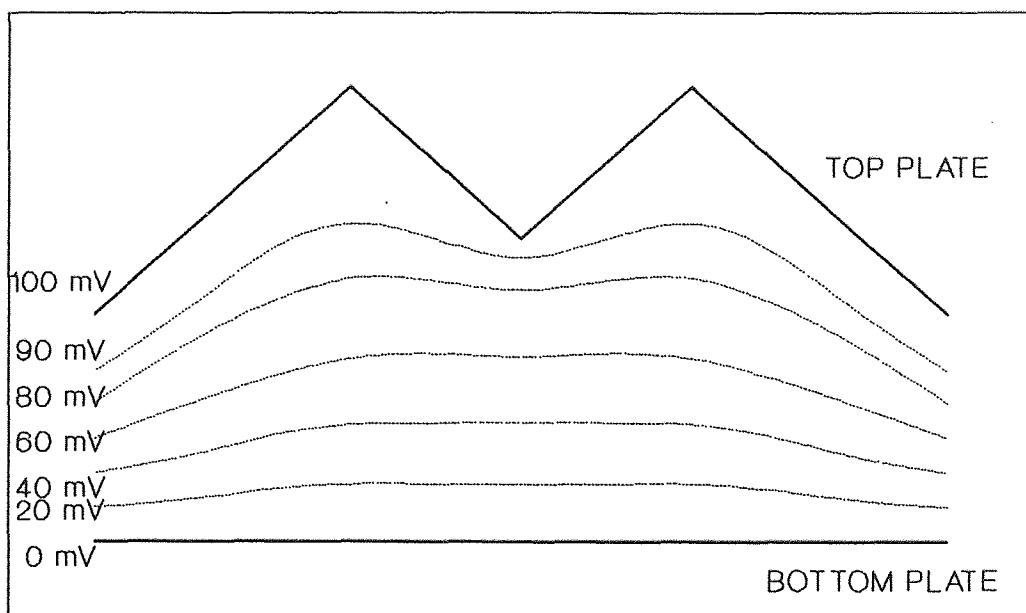


Fig.(6) Equipotential lines for the M-shaped surface cell.

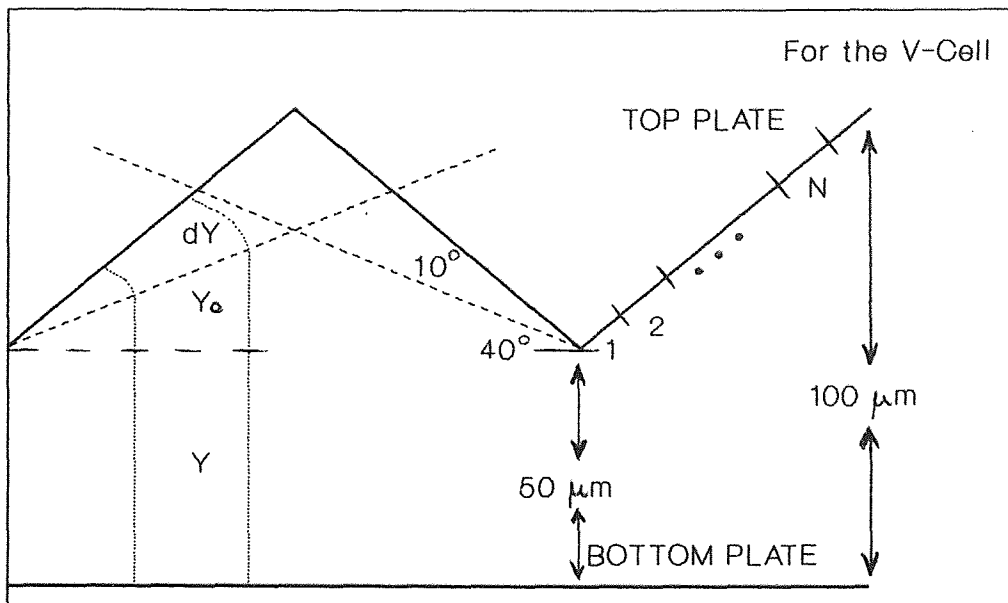


Fig.(7) A comparison between the linear field lines (Y_0 & Y) and the non-linear one (dY).

the field lines is:

$$Y_{Tj} = (Y+Y_{0j}) + dY_j = (50 + \sin(\theta-\theta_0)r_j) + r_j\theta_0 \quad (\mu\text{m}) \quad (29)$$

where: $j = 1, 2, \dots, N$, with N being discrete area sections as shown in Fig.(7). The relationship between the non-linear and the linear parts is shown in Fig.(8). Thus, a correction to the current path is needed to account for the distance between the two conducting plates of the solar cell. A multiplicity factor ξ_j is defined to account for the non-homogeneous current distribution due to non-uniform field distribution. It is defined as follows:

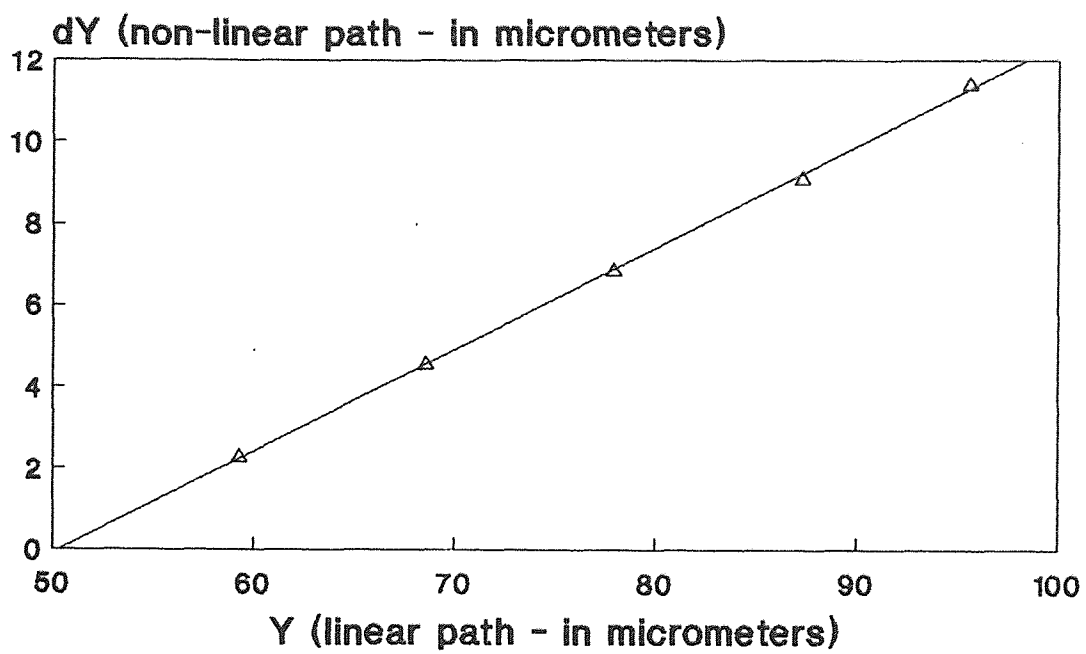
$$\Delta E_j \propto - 1 / Y_{Tj} \quad (30)$$

then the (ξ_j) roughly will be given by (since there is a potential difference between the plates):

$$\xi_j = Y_{T1} / Y_{Tj} \quad (31)$$

where $j = 1, 2, \dots, N$. Figure (9) shows ξ_j vs. total field line length for some of our configurations.

We note, though, that non-homogeneous current distribution is also a result of non-uniform light transmission distribution across the solar cell. This effect will be considered in the next section.



Fig(8) Relation between the linear (Y) and the non-linear (dY) field line paths for the V-shaped surface.

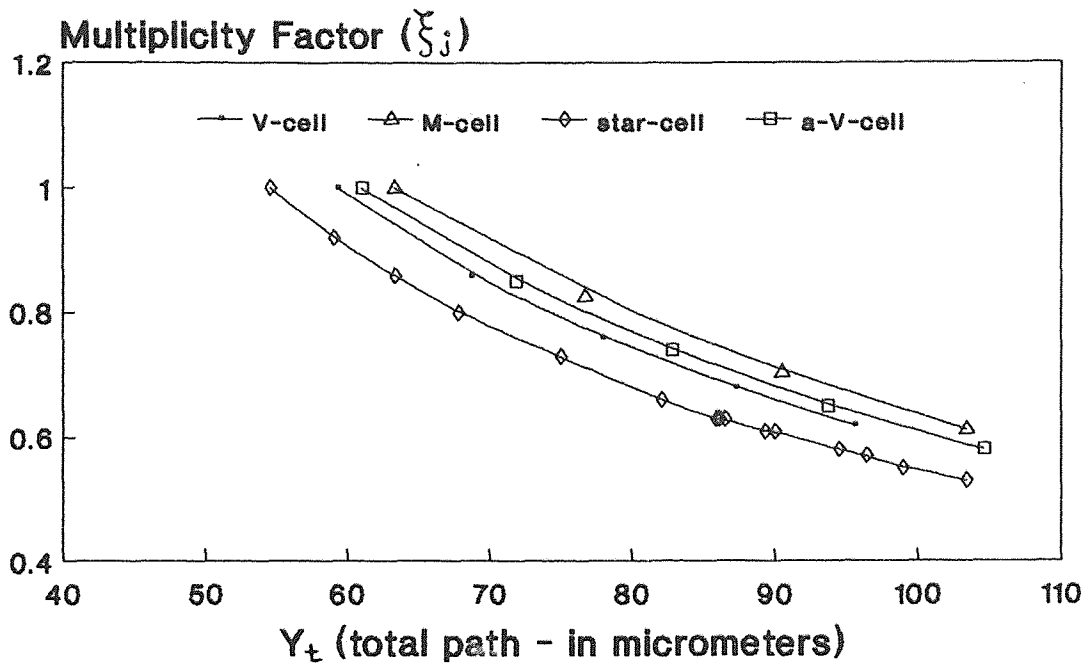


Fig.(9) The multiplicity factor Vs. the total field line path (Y_t).

2.4 The Surface Configurations - Calculations

(a) Flat-surface cells.

Flat Schottky barrier solar cell experiences only one reflection (or transmission). It is found from Eq.(23) that, $R(\lambda) = 0.31$ or $T(\lambda) = 0.69$ (for $n_s=3.5$, at $\lambda=0.9 \mu\text{m}$) and $R(\lambda) = 0.34$ (for $n_s = 4.27$ at $\lambda=0.5 \mu\text{m}$). At $0.9 \mu\text{m}$, substituting the following values:

$$\alpha(\lambda) = 500 \text{ cm}^{-1}$$

$$F = 1.4 \times 10^{18} \text{ photons/ cm}^2 \text{ sec bandwidth}$$

$$W = 2.5 \times 10^{-4} \text{ cm}$$

$$L_p = 20 \times 10^{-4} \text{ cm}$$

$$q = 1.6 \times 10^{-19} \text{ cb}$$

and the use of equations (2) and (17) we get:

$$J_d(\lambda) = 1.82 \times 10^{-4} \text{ A/cm}^2$$

$$J_b(\lambda) = 6.84 \times 10^{-4} \text{ A/cm}^2$$

From Eq.(1.1), we find that:

$$J_L(\lambda) = 8.66 \times 10^{-4} \text{ A/cm}^2$$

as the total photocurrent density.

Assuming flat surface area of $A = 1 \text{ cm}^2$ (which will be the case in all of our calculations) we get:

$$I_L = 8.66 \times 10^{-4} \text{ A}$$

The saturation current is found from Eq.(18) with the

following parameters:

$$A = 1 \text{ cm}^2$$

$$A^{**} = 110 \text{ A/cm}^2/\text{K} \text{ (Richardson constant for n-type)}$$

$$T = 300^\circ \text{ K}$$

$$q\Phi_{Bn} = 2/3 E_g = 1.2 \times 10^{-19} \text{ J}$$

$$K = 1.38 \times 10^{-23} \text{ J/K} \text{ (Boltzmann's constant)}$$

$$I_s = 2.55 \times 10^{-6} \text{ A.}$$

The I-V characteristic can be found from Eq.(19) and is shown in Fig.(24).

At 0.5 μm , with the following parameters,

$$\alpha(\lambda) = 10000 \text{ cm}^{-1}$$

$$F = 1.8 \times 10^{18} \text{ photons/cm}^2 \text{ sec bandwidth}$$

$$W = 2.5 \times 10^{-4} \text{ cm}$$

$$L_p = 20 \times 10^{-4} \text{ cm}$$

we get:

$$J_d(\lambda) = 1.63 \times 10^{-3} \text{ A/cm}^2$$

$$J_b(\lambda) = 1.384 \times 10^{-4} \text{ A/cm}^2$$

$$I_L(\lambda) = 1.77 \times 10^{-3} \text{ A.}$$

The I-V characteristic is shown in Fig.(25).

(b) V-shaped Surface Cells

More than one reflections, before light escapes back to space, can be captured by a grooved surface in a shape of

V-grooves. It is found by a ray tracing method, that, the steeper the sides become, the more reflections we may get, as shown in Figures (10), (11), and (12) versus depth - with $y=0$ taken at the bottom of the grooves. Figure (13) is showing the amount of light transmitted into the cell vs. depth for a 50° front surface slope from the horizontal accounting for the transmittance as discussed by equations (27) and (28). Also shown is the best fit curve. Our calculations showed that 50° sloped surface is an optimum angle from light transmission point of view (V-cell) (see also Refs. [6], [8]). The ray tracing for this case can be seen in Fig. (14), where the light hits the surface at $\theta = 50^\circ$ (incoming perpendicular to the back surface). Two reflections are possible before light escapes back to space, with $\theta_1 = 50^\circ$, $\varphi_1 = 12.6^\circ$, $R_1 = 0.468$ (first reflection) and $\theta_2 = 30^\circ$, $\varphi_2 = 8.2^\circ$, $R_2 = 0.361$ (second reflection), at $0.9 \mu\text{m}$. The $\alpha_1(\lambda, \varphi)$, $\alpha_2(\lambda, \varphi)$, $W_1(\varphi)$, $W_2(\varphi)$ parameters are calculated as indicated by Eqs.(3) and (4) respectively, and the number of incident photons available for the second reflection F_2 is calculated using Eq. (27).

In general the photocurrent will be given by:

$$I_L = \left[\sum_j^N (J_a \Delta A_j)(\xi_j) \right] m + \left[\sum_j^N (J_b \Delta A_j)(\xi_j) \right] m \quad (32)$$

where: $j = 1, 2, \dots, N$

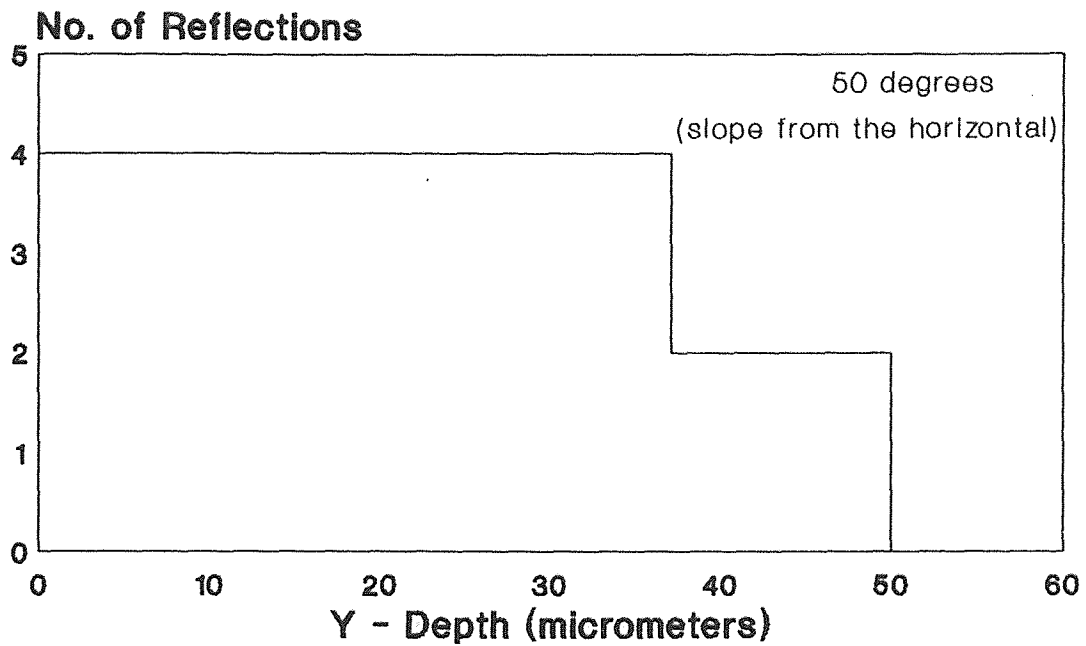


Fig.(10) No. of Reflections per V aperture Vs. depth for the V-shaped surface.

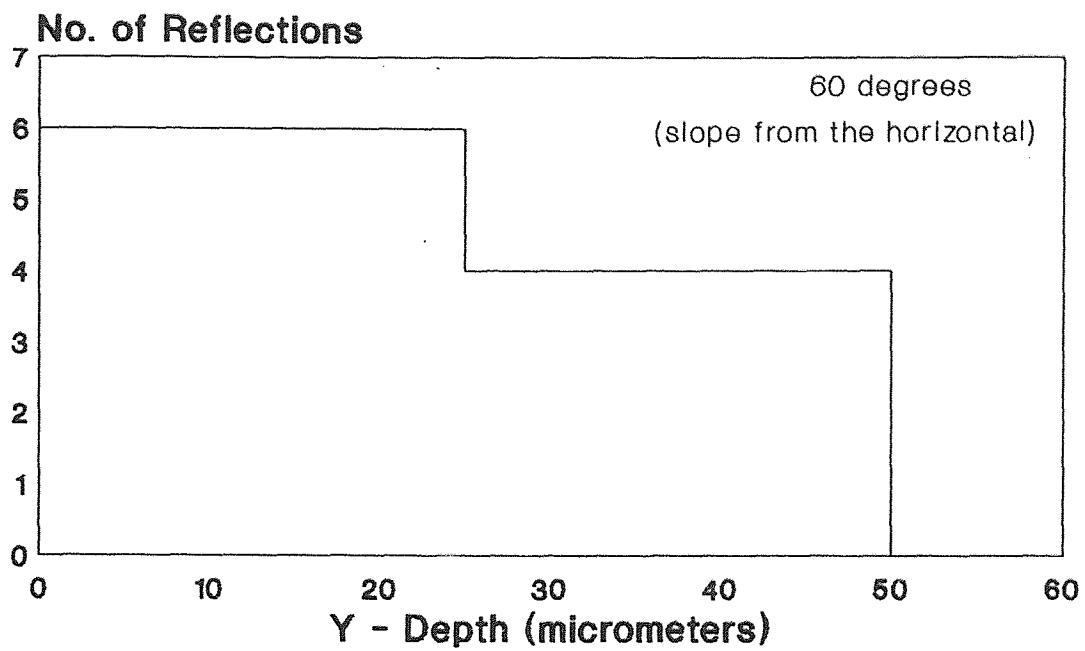


Fig.(11) Number of Reflections per V aperture Vs. depth for the V-shaped surface.

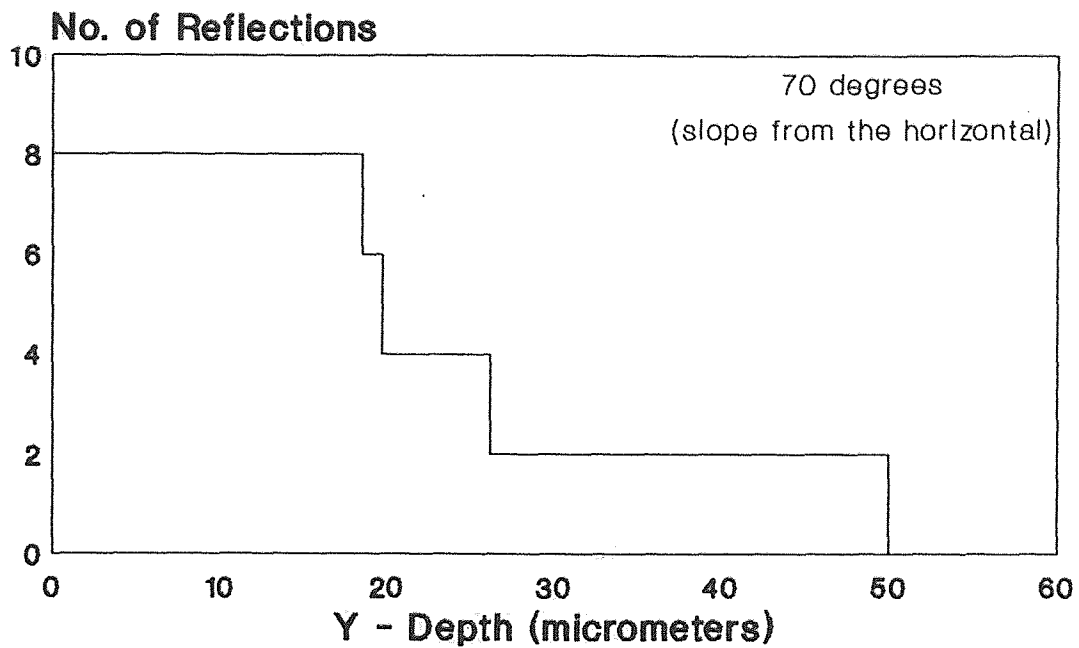


Fig.(12) Number of Reflections per V aperture Vs. depth for the V-shaped surface.

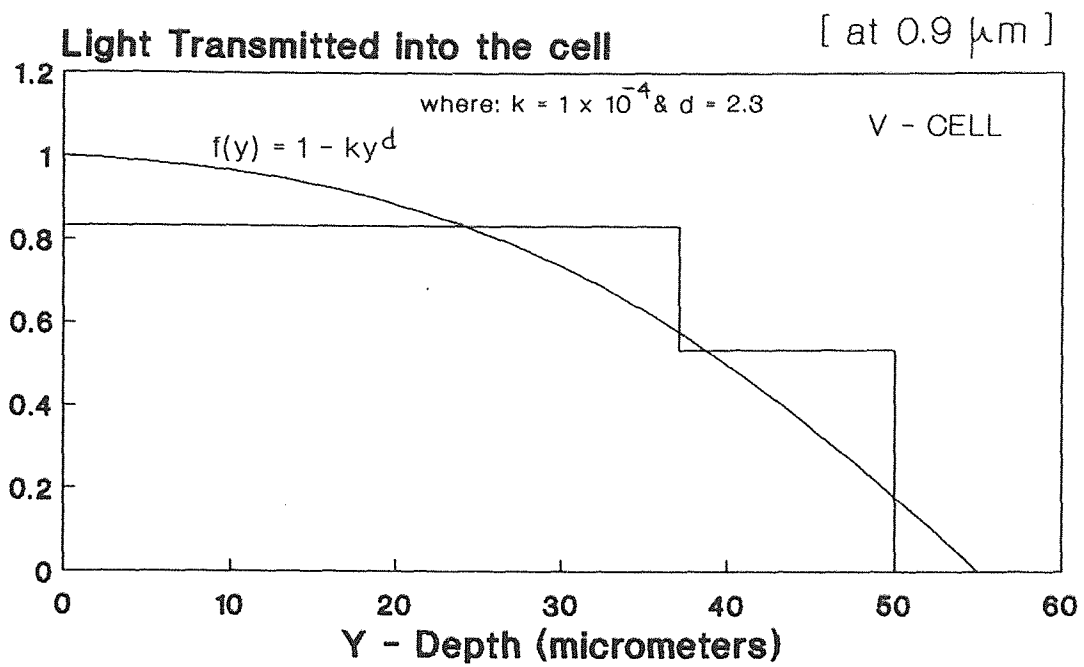


Fig.(13) Amount of light Transmitted into the cell (per unit V) for the V-shaped surface.

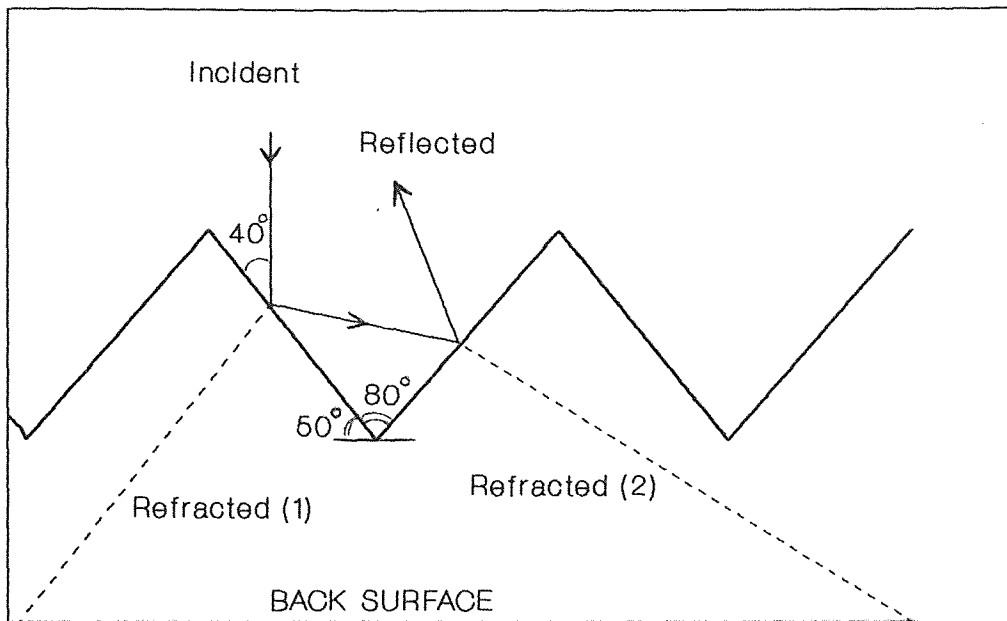


Fig.(14) The V-shaped surface cell (50°)

N -- is the number of sections of the surface,
 m -- is the number of sides in a unit cell- $m = \tan(\theta)/\Psi$
 where Ψ is the amplitude of pattern.

ΔA_j -- is the area (unit area) of each section,

ξ_j -- is the multiplicity factor as discussed above
 and shown in Fig. (9) - usually takes values
 form 1.0 to 0.5 .

If we assume $N = 5$ for simplicity, we find using appendix B,
 at $\lambda = 0.9 \mu\text{m}$, that: (first reflection) -

$$I_{d1} = \left[\sum_j^N (J_{d1} \Delta A_j) (\xi_j) \right] m = 1.75 \times 10^{-4} \text{ A}$$

$$I_{b1} = \left[\sum_j^N (J_{b1} \Delta A_j) (\xi_j) \right] m = 6.32 \times 10^{-4} \text{ A}$$

-(second reflection)-

$$I_{d2} = \left[\sum_j^N (J_{d2} \Delta A_j) (\xi_j) \right] m = 7.72 \times 10^{-5} \text{ A}$$

$$I_{b2} = \left[\sum_j^N (J_{b2} \Delta A_j) (\xi_j) \right] m = 2.85 \times 10^{-4} \text{ A}$$

Finally we get:

$$I_L = I_{d1} + I_{b1} + I_{d2} + I_{b2} = 1.17 \times 10^{-3} \text{ A}$$

Using Eq. (18) with same values as before, (accounting for
 the area):

$$A = \tan(50)/\sin(50) = 1.555 \text{ cm}^2$$

so: $I_s = 4.09 \times 10^{-8} \text{ A}$.

The I-V characteristic can be seen in Fig.(24).

At $\lambda = 0.5 \mu\text{m}$, we get:

$$I_{d1} = 1.46 \times 10^{-3} \text{ A},$$

$$I_{b1} = 1.14 \times 10^{-4} \text{ A},$$

$$I_{d2} = 7.9 \times 10^{-4} \text{ A},$$

$$I_{b2} = 6.47 \times 10^{-5} \text{ A},$$

and, $I_L = 2.43 \times 10^{-3} \text{ A}$.

The I-V characteristic is shown in Fig.(25).

(c) Star-shaped Surface cells and the Inverted-Star surface cells

In the Star-shaped surface cell we divided each side into four regions (A_1, A_2, A_3, A_4) as shown in Fig.(15). Each one of these regions has the following area values:

$$A_1 = A_4 = 21.76 \times 10^{-4} \text{ cm}^2$$

$$A_2 = A_3 = 16.93 \times 10^{-4} \text{ cm}^2$$

The number of sides (m) is kept the same as for the V-shaped to be $m = 238 \text{ sides/cm}^2$. So the total surface area for star-shaped cell will be given by:

$$A = (A_1 + A_2 + A_3 + A_4)m = 1.84 \text{ cm}^2$$

The reflections are listed as follows:

In A_1 : A 1st reflection over the entire area ($\theta_1=50^\circ$);

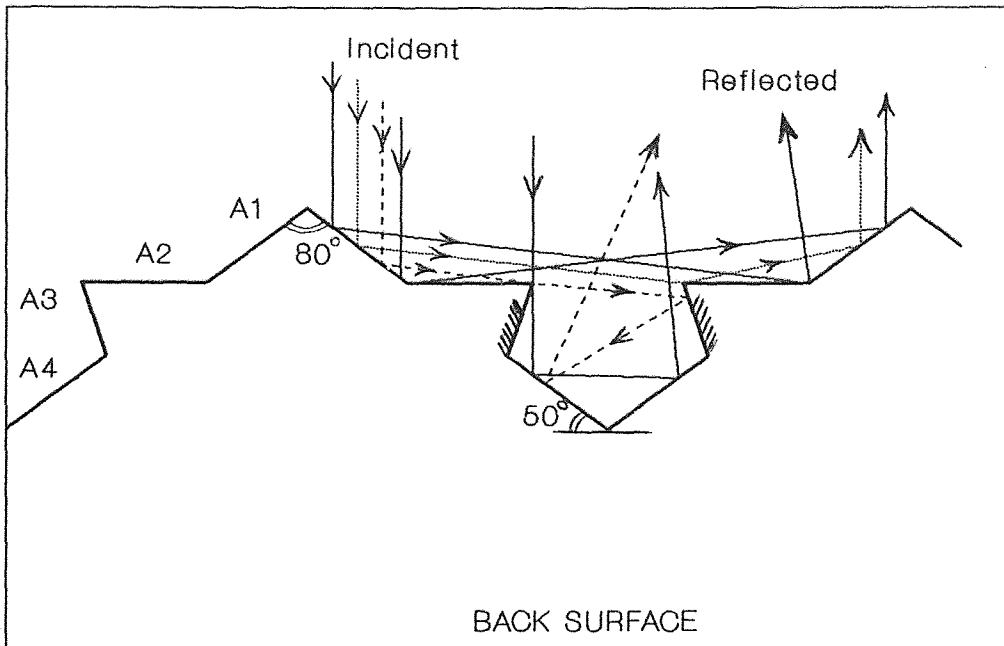


Fig.(15) The Star-shaped surface cell.

A 2nd reflection over the bottom of area A₁ -
in 5 x 10⁻⁴ cm² - (θ₂=30°);

A 3rd reflection over an area between the
10.6 x 10⁻⁴ and the 15.13 x 10⁻⁴ cm² -(θ₃=50°)

in A₂: A 1st reflection over the entire area (θ₁=0°);
two 2nd reflections over the entire area (θ₂=80°),

in A₃: we get only a 2nd reflection over an area of about
4.1 x 10⁻⁴ cm² at the top of A₃ (θ₂=20°)

in A₄: A 1st reflection over an area from the bottom groove
to about 17.2 x 10⁻⁴ cm² up (θ₁=50°);
a 2nd reflection over an area from the bottom groove
to about 12.8 x 10⁻⁴ cm² up (θ₂=30°);
and a 3rd reflection over a region at the top from
17.2 x 10⁻⁴ to 21.76 x 10⁻⁴ cm² (θ₃=10°).

We got the following values, at λ = 0.9 μm, for R, α, and W
per region by using Fig.(2) and Eqs.(3) and (4):

(A₁): R₁^{<1>}=0.466 ; R₂^{<1>}=0.36 ; R₃^{<1>}=0.466
α₁^{<1>}=512.4 cm⁻¹ ; α₂^{<1>}=505.2 cm⁻¹ ; α₃^{<1>}=512.4 cm⁻¹
W₁^{<1>}=2.56 x 10⁻⁴ cm ; W₂^{<1>}=2.53 x 10⁻⁴ cm ;
W₃^{<1>}=2.56 x 10⁻⁴ cm,

(A₂): R₁^{<2>}=0.31 ; R₂^{<2>}=0.813
α₁^{<2>}=500 cm⁻¹ ; α₁^{<2>}=521 cm⁻¹
W₁^{<2>}=2.5 x 10⁻⁴ cm ; W₂^{<2>}=2.6 x 10⁻⁴ cm,

(A₃): R₂^{<3>} = 0.332
α₂^{<3>} = 502.4 cm⁻¹

$$W_2^{(3)} = 2.51 \times 10^{-4}$$

$$(A_4): R_1^{(4)}=0.466 ; R_2^{(4)}=0.36 ; R_3^{(4)}=0.315$$

$$\alpha_1^{(4)}=512.4 \text{ cm}^{-1} ; \alpha_2^{(4)}=505.2 \text{ cm}^{-1} ; \alpha_3^{(4)}=501 \text{ cm}^{-1}$$

$$W_1^{(4)}=2.56 \times 10^{-4} \text{ cm} ; W_2^{(4)}=2.53 \times 10^{-4} \text{ cm} ;$$

$$W_3^{(4)}=2.5 \times 10^{-4} \text{ cm}.$$

Now if we assume for simplicity that we divide each of those areas in four sections (N=4) then the multiplicity factor gets the values:

$$(A_1): \xi_j^{(1)} = 0.61 \text{ to } 0.53$$

$$(A_2): \xi_j^{(2)} = 0.63 \text{ (about constant value)}$$

$$(A_3): \xi_j^{(3)} = 0.73 \text{ to } 0.57$$

$$(A_4): \xi_j^{(4)} = 1.0 \text{ to } 0.8$$

and the photocurrents calculated per region are (at 0.9 μm):

$$\begin{aligned} I_L^{(A_1)} = & \left[\sum_j^N (J_{d1}^{(1)} \Delta A_j^{(1)}) (\xi_j^{(1)}) \right] m + \\ & + \left[\sum_j^N (J_{b1}^{(1)} \Delta A_j^{(1)}) (\xi_j^{(1)}) \right] m + \\ & + \left[\sum_j^{N'} (J_{d2}^{(1)} \Delta A_j^{(1)}) (\xi_j^{(1)}) \right] m + \\ & + \left[\sum_j^{N'} (J_{b2}^{(1)} \Delta A_j^{(1)}) (\xi_j^{(1)}) \right] m + \\ & + \left[\sum_j^{N''} (J_{d3}^{(1)} \Delta A_j^{(1)}) (\xi_j^{(1)}) \right] m + \\ & + \left[\sum_j^{N''} (J_{b3}^{(1)} \Delta A_j^{(1)}) (\xi_j^{(1)}) \right] m = \\ & = [1.83 \times 10^{-7} \text{ A/side} + 6.6 \times 10^{-7} \text{ A/side} + \\ & + 2.45 \times 10^{-8} \text{ A/side} + 9.0 \times 10^{-8} \text{ A/side} + \end{aligned}$$

$$\begin{aligned}
& + 1.36 \times 10^{-8} \text{ A/side} + 5.0 \times 10^{-8} \text{ A/side}] m = \\
= & (1.02 \times 10^{-8} \text{ A/side}) (238 \text{ sides}) = \\
= & 2.43 \times 10^{-4} \text{ A.}
\end{aligned}$$

$$\begin{aligned}
I_{L(A2)} = & [\sum_j^N (J_{d1}^{(2)} \Delta A_j^{(2)}) (\xi_j^{(2)})] m + \\
& + [\sum_j^N (J_{b1}^{(2)} \Delta A_j^{(2)}) (\xi_j^{(2)})] m + \\
& + [2 \sum_j^N (J_{d2}^{(2)} \Delta A_j^{(2)}) (\xi_j^{(2)})] m + \\
& + [2 \sum_j^N (J_{b2}^{(2)} \Delta A_j^{(2)}) (\xi_j^{(2)})] m = \\
= & [1.94 \times 10^{-7} \text{ A/side} + 7.3 \times 10^{-7} \text{ A/side} + \\
& + 2(1.76 \times 10^{-8} \text{ A/side}) + 2(1.36 \times 10^{-7} \text{ A/side})] m = \\
= & (1.23 \times 10^{-6} \text{ A/side})(238 \text{ sides}) = \\
= & 2.93 \times 10^{-4} \text{ A.}
\end{aligned}$$

$$\begin{aligned}
I_{L(A3)} = & [\sum_j^{N'} (J_{d2}^{(3)} \Delta A_j^{(3)}) (\xi_j^{(3)})] m + \\
& + [\sum_j^{N'} (J_{b2}^{(3)} \Delta A_j^{(3)}) (\xi_j^{(3)})] m = \\
= & [1.94 \times 10^{-8} \text{ A/side} + 6.92 \times 10^{-8} \text{ A/side}] m = \\
= & (8.86 \times 10^{-8}) (238) = \\
= & 2.11 \times 10^{-5} \text{ A.}
\end{aligned}$$

$$\begin{aligned}
I_{L(A4)} = & [\sum_j^N (J_{d1}^{(4)} \Delta A_j^{(4)}) (\xi_j^{(4)})] m + \\
& + [\sum_j^N (J_{b1}^{(4)} \Delta A_j^{(4)}) (\xi_j^{(4)})] m +
\end{aligned}$$

$$\begin{aligned}
& + \left[\sum_j^{N'} (J_{d2}^{(4)} \Delta A_j^{(4)}) (\xi_j^{(4)}) \right] m + \\
& + \left[\sum_j^{N'} (J_{b2}^{(4)} \Delta A_j^{(4)}) (\xi_j^{(4)}) \right] m + \\
& + \left[\sum_j^{N''} (J_{d3}^{(4)} \Delta A_j^{(4)}) (\xi_j^{(4)}) \right] m + \\
& + \left[\sum_j^{N''} (J_{b3}^{(4)} \Delta A_j^{(4)}) (\xi_j^{(4)}) \right] m = \\
& = [1.08 \times 10^{-8} \text{ A/side} + 4.53 \times 10^{-7} \text{ A/side} + \\
& + 5.25 \times 10^{-8} \text{ A/side}] m = \\
& = (1.584 \times 10^{-8} \text{ A/side}) (238 \text{ side}) = \\
& = 3.77 \times 10^{-4} \text{ A},
\end{aligned}$$

therefore the total photocurrent will be given by:

$$I_L = I_L^{(A1)} + I_L^{(A2)} + I_L^{(A3)} + I_L^{(A4)} = 9.34 \times 10^{-4} \text{ A}.$$

Some of the above values were also tested by the computer program in appendix B region by region.

By using $A = 1.84 \text{ cm}^2$ and keeping the remaining values unchanged, we get from Eq.(18):

$$I_s = 4.7 \times 10^{-6} \text{ A}$$

The I-V characteristic is shown in Fig. (24).

At, $\lambda = 0.5 \mu\text{m}$, we get:

$$I_L^{(A1)} = (2.22 \times 10^{-8} \text{ A/side})(238 \text{ sides}) = 0.528 \times 10^{-3} \text{ A}$$

$$I_L^{(A2)} = (2.23 \times 10^{-6} \text{ A/side})(238 \text{ sides}) = 0.531 \times 10^{-3} \text{ A}$$

$$I_L^{(A3)} = (2.07 \times 10^{-7} \text{ A/side})(238 \text{ sides}) = 4.92 \times 10^{-5} \text{ A}$$

$I_L(A^4) = (3.36 \times 10^{-6} \text{ A/side})(238 \text{ sides}) = 0.80 \times 10^{-3} \text{ A}$
and, $I_L = 1.91 \times 10^{-3} \text{ A}$.

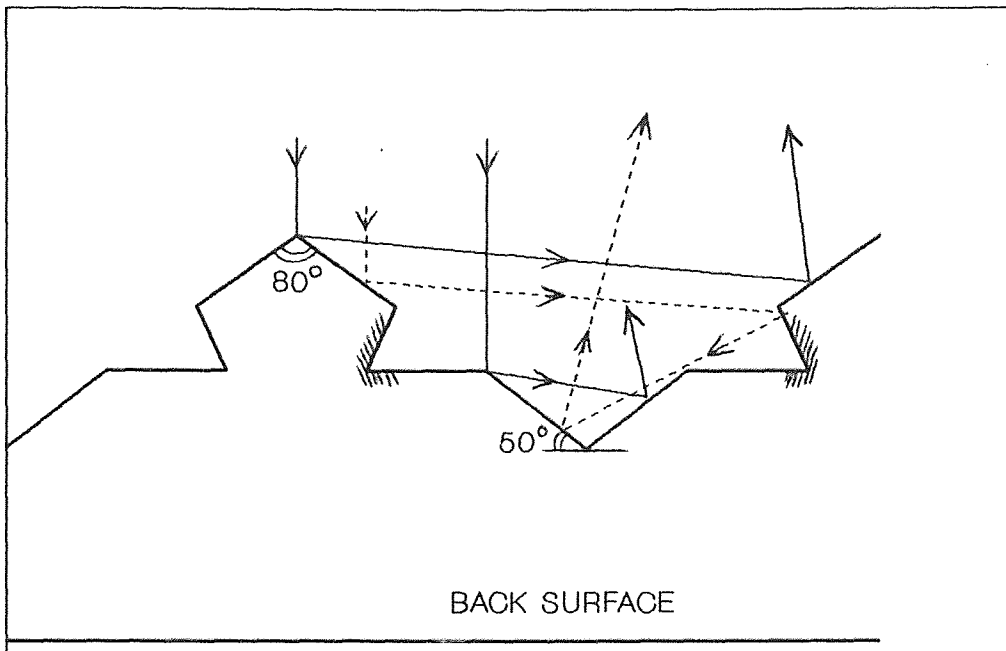
The I-V characteristic is shown in Fig.(25).

As we see here we do not get much of an improvement for this kind of surface configuration primarily due to creation of a dark area(light never gets there), shown as shades in Fig.(15), and as a result, only very little current is drawn out of that region (only 2.26 % of the total).

With the same analogy as for this star-shaped surface the Inverted-star-shaped surface cell shown in Fig. (16) was tested and found, like the star, showing not much of an improvement over the V-cell having its I-V characteristic curve falling in the same region that the star's does. The "dark" areas are shown in Fig.(16) as the shaded ones.

(d) The M-shaped Surface Cell.

This surface configuration is shown in Fig. (17). In Figs. (18) and (19) we show the number of reflections and the light transmitted into the cell vs. depth respectively. For simplicity we assume two regions, A_1 and A_2 shown in Fig.(17) with each one having an area of: $A_1 = 32.63 \times 10^{-4} \text{ cm}^2/\text{side}$ and $A_2 = 2(A_1) = 65.3 \times 10^{-4} \text{ cm}^2/\text{side}$, totaling 159 sides ($m = 159$) per unit cell. The total area is found to be: $A=1.557 \text{ cm}^2$. The values for α , R , W are the same for 1st



Fig(16) The Inverted-star-shaped surface

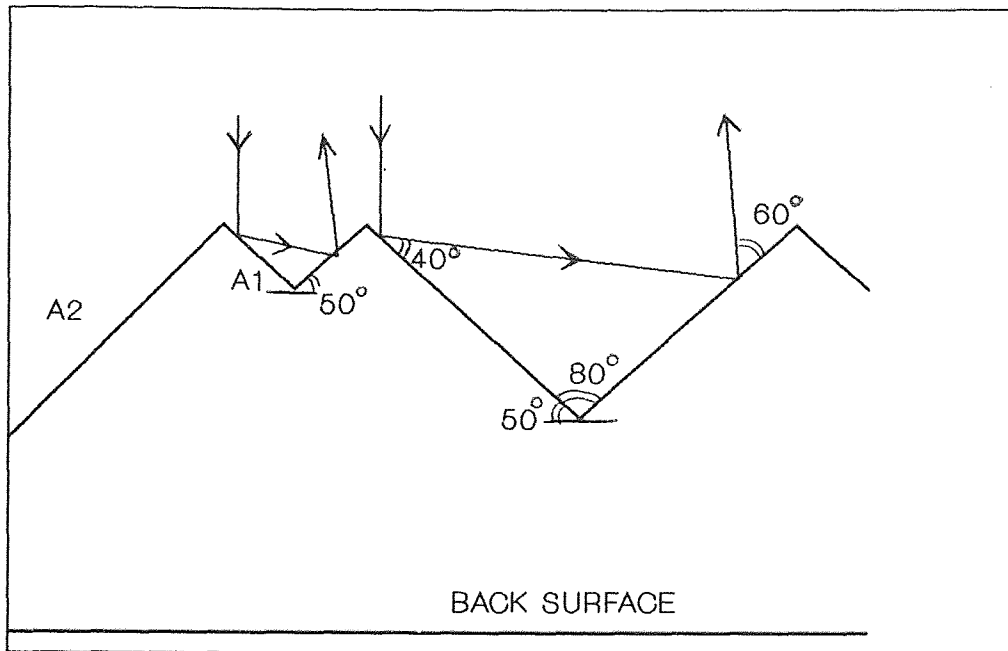


Fig.(17) The M-shaped surface cell

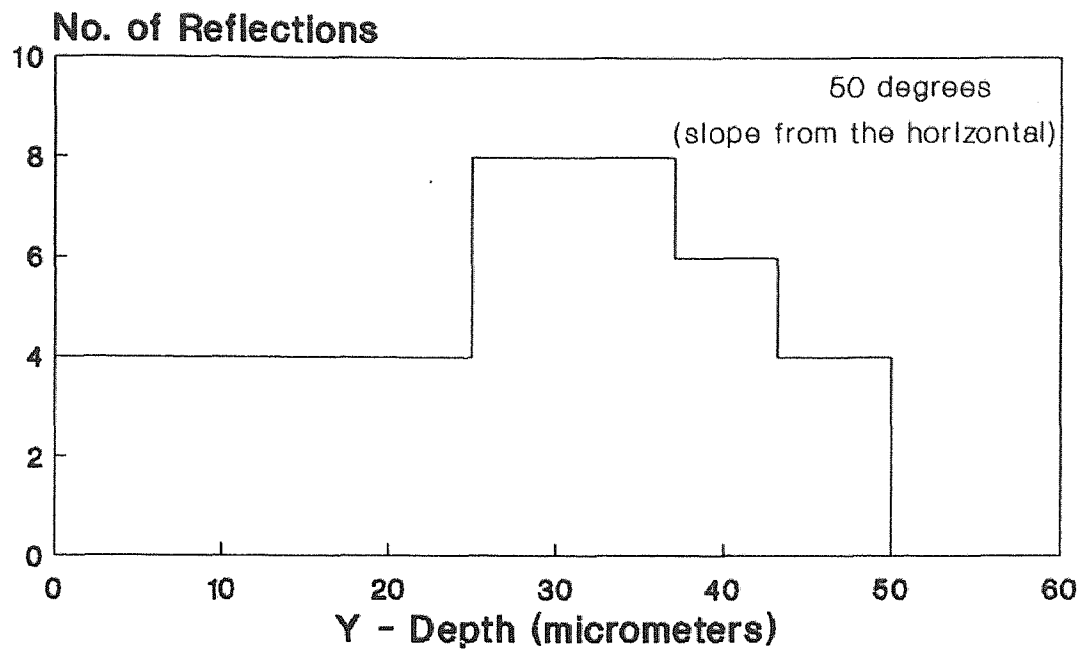


Fig.(18) Number of Reflections per M aperture Vs. depth for the M-shaped surface.

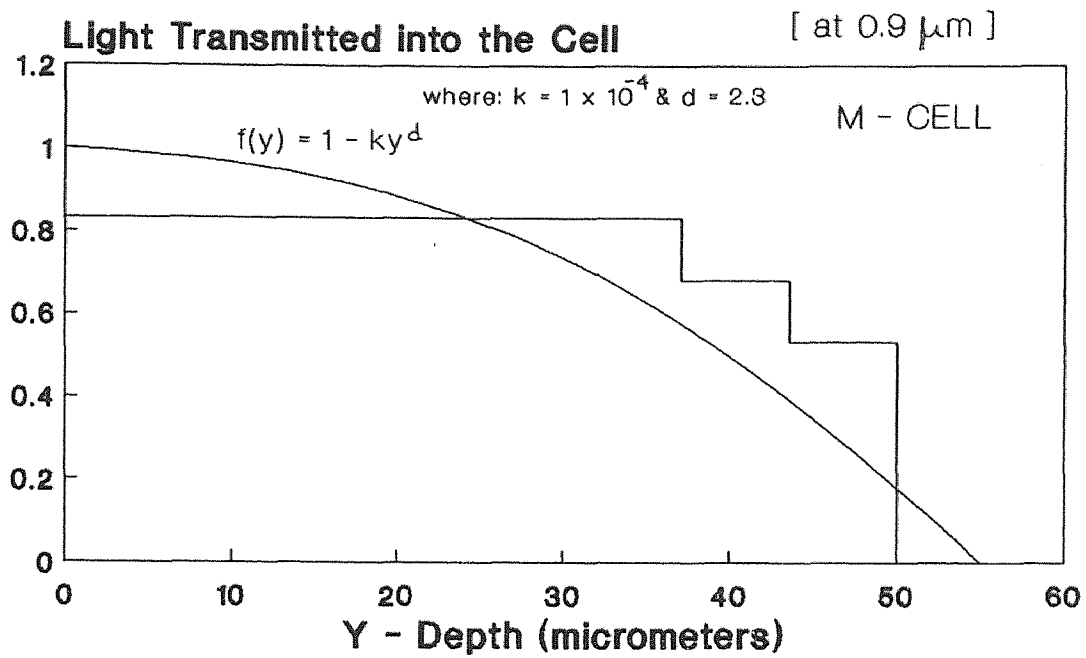


Fig.(19) Amount of light Transmitted into the cell (per unit M) for the M-shaped surface.

and 2nd reflections as indicated in the V-shaped surface. The (ξ_j) for A_2 is practically the same as for the V-shaped cell, but for A_1 it shows a little bit of improvement.

As before, at $\lambda = 0.9 \mu\text{m}$, the photocurrent will be given by:

$$\begin{aligned}
 I_L^{(A1)} &= \left\{ \sum_j^N [(J_{d1}^{(1)} \Delta A_j^{(1)}) (\xi_j^{(1)}) + (J_{b1}^{(1)} \Delta A_j^{(1)}) (\xi_j^{(1)})] \right\} m + \\
 &+ \left\{ \sum_j^{N'} [(J_{d2}^{(1)} \Delta A_j^{(1)}) (\xi_j^{(1)}) + (J_{b2}^{(1)} \Delta A_j^{(1)}) (\xi_j^{(1)})] \right\} m = \\
 &= \{ 4.1 \times 10^{-7} \text{ A/side} + 1.48 \times 10^{-6} \text{ A/side} + \\
 &+ 1.68 \times 10^{-7} \text{ A/side} + 6.2 \times 10^{-7} \text{ A/side} \} m = \\
 &= \{ 2.678 \times 10^{-6} \text{ A/side} \} (159 \text{ sides}) = \\
 &= 4.25 \times 10^{-4} \text{ A.}
 \end{aligned}$$

$$\begin{aligned}
 I_L^{(A2)} &= \left\{ \sum_j^N [(J_{d1}^{(2)} \Delta A_j^{(2)}) (\xi_j^{(2)}) + (J_{b1}^{(2)} \Delta A_j^{(2)}) (\xi_j^{(2)})] \right\} m + \\
 &+ \left\{ \sum_j^{N'} [(J_{d2}^{(2)} \Delta A_j^{(2)}) (\xi_j^{(2)}) + (J_{b2}^{(2)} \Delta A_j^{(2)}) (\xi_j^{(2)})] \right\} m = \\
 &= \{ 7.6 \times 10^{-7} \text{ A/side} + 2.73 \times 10^{-6} \text{ A/side} + \\
 &+ 3.33 \times 10^{-7} \text{ A/side} + 1.22 \times 10^{-6} \text{ A/side} \} m = \\
 &= \{ 5.04 \times 10^{-6} \text{ A/side} \} (159 \text{ sides}) = \\
 &= 8.0 \times 10^{-4} \text{ A}
 \end{aligned}$$

and the total photocurrent is given by:

$$\begin{aligned}
 I_L &= I_L^{(A1)} + I_L^{(A2)} = 4.25 \times 10^{-4} + 8.0 \times 10^{-4} \text{ A} = \\
 &= 1.22 \times 10^{-3} \text{ A.}
 \end{aligned}$$

The saturation current I_s remains the same as in the V-shaped

surface to be:

$$I_s = 4.09 \times 10^{-6} \text{ A.}$$

From Eq.(19) we can get the I-V characteristic for the M-shaped surface which is shown in figure (24).

At, $\lambda = 0.5 \mu\text{m}$, we get:

$$I_{d1}(A1) = 3.4 \times 10^{-6} \text{ A/side,}$$

$$I_{b1}(A1) = 2.65 \times 10^{-7} \text{ A/side,}$$

$$I_{d1}(A2) = 6.31 \times 10^{-6} \text{ A/side,}$$

$$I_{b1}(A2) = 4.9 \times 10^{-7} \text{ A/side,}$$

$$I_{d2}(A1) = 1.69 \times 10^{-6} \text{ A/side,}$$

$$I_{b2}(A1) = 1.40 \times 10^{-7} \text{ A/side,}$$

$$I_{d2}(A2) = 3.32 \times 10^{-6} \text{ A/side,}$$

$$I_{b2}(A2) = 2.75 \times 10^{-7} \text{ A/side,}$$

and finally:

$$I_L = (1.59 \times 10^{-5} \text{ A/side})(159 \text{ sides}) = 2.53 \times 10^{-3} \text{ A.}$$

The I-V characteristic is shown in Fig.(25).

The little improvement that we get over the V-shaped cell is primarily due to electrical and not really to optical advancement.

(e) Asymmetric V-shaped Surface Cells

Another kind of V-cell is presented here, with the difference that the two sides are unequal by changing the

angle of elevation over the horizontal. This asymmetric V-shaped surface is shown in figure (20). We can see that the two angles formed over the horizontal at the low grooves are of 50° and 70° respectively. The number of reflections and the amount of light transmitted into the cell vs. depth are shown in figures (21) and (22). On each of these sides we get three reflections before light escapes. For simplicity again let's call A_1 the region with the 50° elevation and A_2 the region with 70° elevation.

It is found that: $A_1 = (50 \mu\text{m} / \sin(50))(1 \text{ cm}^2) =$
 $= 65.3 \times 10^{-4} \text{ cm}^2$

$$A_2 = (50 \mu\text{m} / \sin(70))(1 \text{ cm}^2) =$$

$$= 53.2 \times 10^{-4} \text{ cm}^2$$

and with 166 sides over a flat area of 1 cm^2 , ($m = 166$) the total area for such surface will be:

$$A = (A_1 + A_2) (166) = 1.97 \text{ cm}^2.$$

Our parameters for each side, at $\lambda = 0.9 \mu\text{m}$, are found to be:

In (A_1): $R_1^{(1)}=0.468$; $R_2^{(1)}=0.314$; $R_3^{(1)}=0.665$
 $\alpha_1^{(1)}=512.4 \text{ cm}^{-1}$; $\alpha_2^{(1)}=501 \text{ cm}^{-1}$; $\alpha_3^{(1)}=519 \text{ cm}^{-1}$
 $W_1^{(1)}=2.56 \times 10^{-4} \text{ cm}$; $W_2^{(1)}=2.5 \times 10^{-4} \text{ cm}$;
 $W_3^{(1)}=2.59 \times 10^{-4} \text{ cm}.$

In (A_2): $R_1^{(2)}=0.665$; $R_2^{(2)}=0.314$; $R_3^{(2)}=0.468$
 $\alpha_1^{(2)}=519 \text{ cm}^{-1}$; $\alpha_2^{(2)}=501 \text{ cm}^{-1}$; $\alpha_3^{(2)}=512.4 \text{ cm}^{-1}$
 $W_1^{(2)}=2.59 \times 10^{-4} \text{ cm}$; $W_2^{(2)}=2.5 \times 10^{-4} \text{ cm}$;

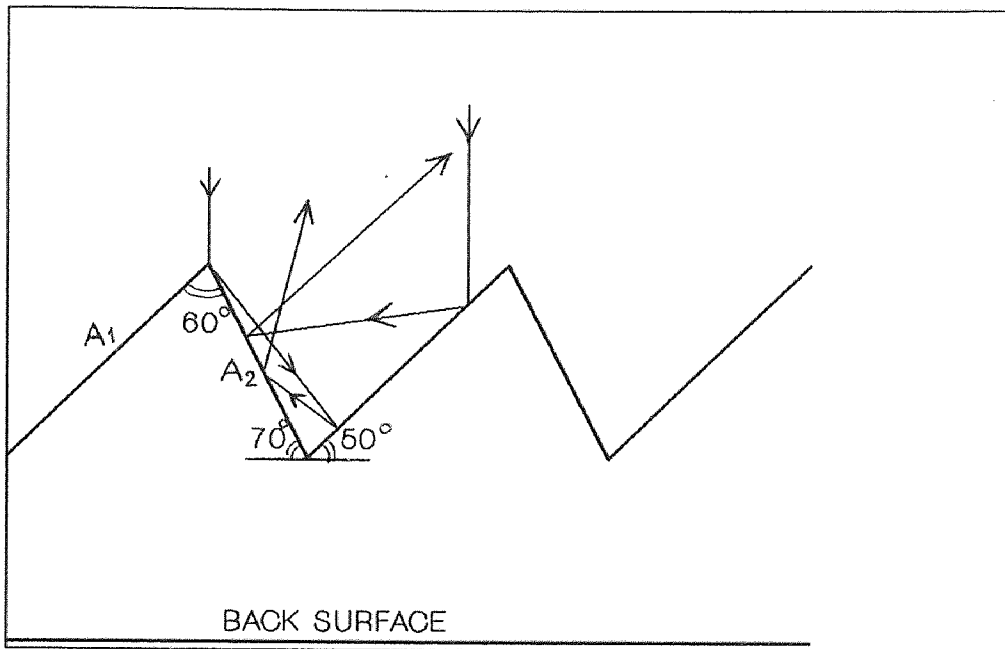


Fig.(20) The Asymmetric-V-shaped surface

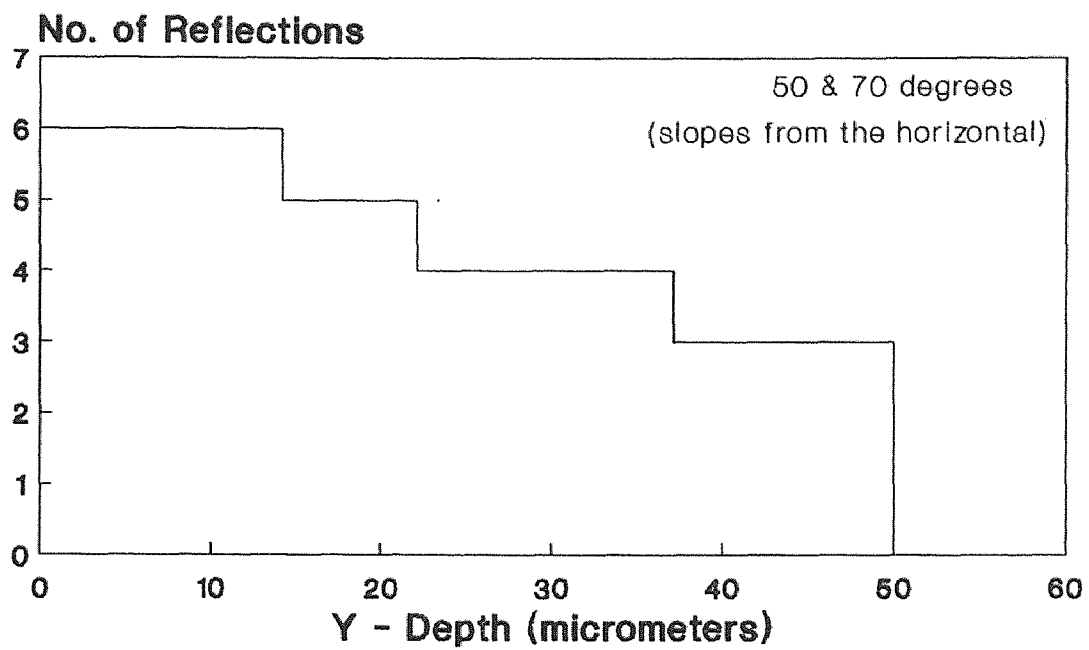


Fig.(21) Number of Reflections per A-V aperture Vs. depth for the Asymmetric V shaped surface.

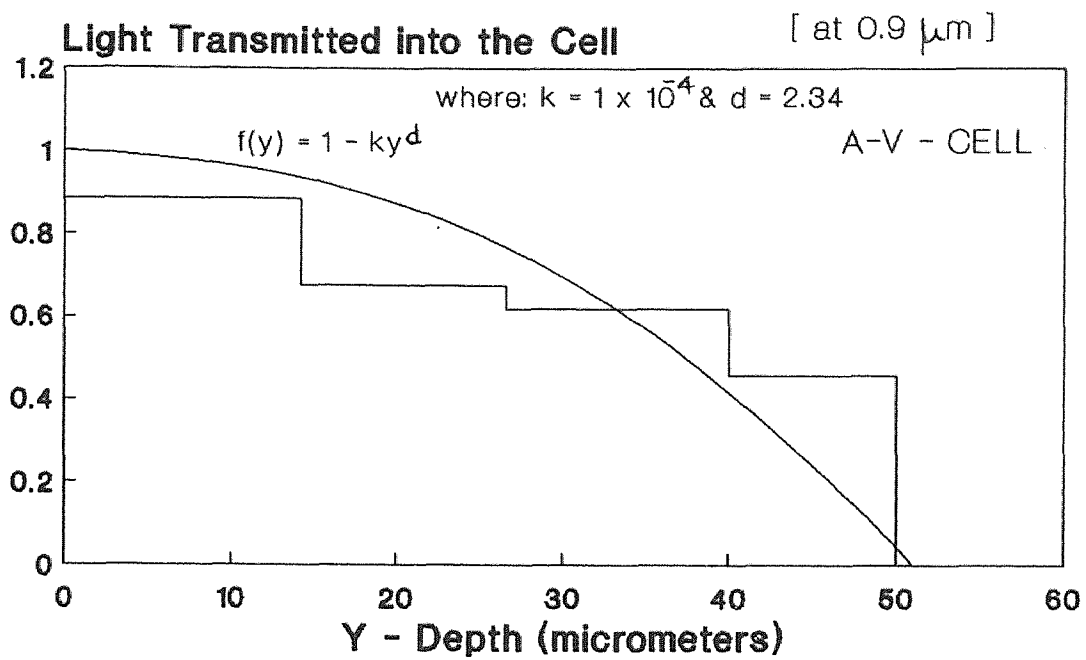


Fig.(22) Amount of light Transmitted into the cell (per unit V) for the asymmetric-V-shaped surface.

$$W_3\langle 2 \rangle = 2.56 \times 10^{-4} \text{ cm.}$$

In evaluating the multiplicity factor (ξ_j) for the A_1 side, θ_0 in equation (29) is taken to be 15° while for the A_2 is taken to be 20° because this side is more steeper than A_1 . Then ξ_j is taking values from 1.0 to 0.57 for both sides as shown in figure (9), with a number of sections equal to five ($N = 5$). Therefore, the photocurrents generated, at $0.9 \mu\text{m}$, are:

$$\begin{aligned} I_{L\langle A1 \rangle} &= \left\{ \sum_j^N [(J_{d1}\langle 1 \rangle \Delta A_j \langle 1 \rangle) (\xi_j \langle 1 \rangle) + (J_{b1}\langle 1 \rangle \Delta A_j \langle 1 \rangle) (\xi_j \langle 1 \rangle)] \right\} m + \\ &+ \left\{ \sum_j^{N'} [(J_{d2}\langle 1 \rangle \Delta A_j \langle 1 \rangle) (\xi_j \langle 1 \rangle) + (J_{b2}\langle 1 \rangle \Delta A_j \langle 1 \rangle) (\xi_j \langle 1 \rangle)] \right\} m + \\ &+ \left\{ \sum_j^{N''} [(J_{d3}\langle 1 \rangle \Delta A_j \langle 1 \rangle) (\xi_j \langle 1 \rangle) + (J_{b3}\langle 1 \rangle \Delta A_j \langle 1 \rangle) (\xi_j \langle 1 \rangle)] \right\} m = \\ &= \{ 7.3 \times 10^{-7} \text{ A/side} + 2.65 \times 10^{-8} \text{ A/side} \} m + \\ &+ \{ 2.13 \times 10^{-7} \text{ A/side} + 8.0 \times 10^{-7} \text{ A/side} \} m + \\ &+ \{ 6.8 \times 10^{-8} \text{ A/side} + 2.45 \times 10^{-7} \text{ A/side} \} m = \\ &= \{ 4.706 \times 10^{-8} \text{ A/side} \} (166 \text{ sides}) = \\ &= 7.81 \times 10^{-4} \text{ A} \end{aligned}$$

$$\begin{aligned} I_{L\langle A2 \rangle} &= \left\{ \sum_j^N [(J_{d1}\langle 2 \rangle \Delta A_j \langle 2 \rangle) (\xi_j \langle 2 \rangle) + (J_{b1}\langle 2 \rangle \Delta A_j \langle 2 \rangle) (\xi_j \langle 2 \rangle)] \right\} m + \\ &+ \left\{ \sum_j^{N'} [(J_{d2}\langle 2 \rangle \Delta A_j \langle 2 \rangle) (\xi_j \langle 2 \rangle) + (J_{b2}\langle 2 \rangle \Delta A_j \langle 2 \rangle) (\xi_j \langle 2 \rangle)] \right\} m + \\ &+ \left\{ \sum_j^{N''} [(J_{d3}\langle 2 \rangle \Delta A_j \langle 2 \rangle) (\xi_j \langle 2 \rangle) + (J_{b3}\langle 2 \rangle \Delta A_j \langle 2 \rangle) (\xi_j \langle 2 \rangle)] \right\} m = \\ &= \{ 3.775 \times 10^{-7} \text{ A/side} + 1.34 \times 10^{-8} \text{ A/side} \} m + \end{aligned}$$

$$\begin{aligned}
& + \{ 2.885 \times 10^{-7} \text{ A/side} + 1.1 \times 10^{-8} \text{ A/side} \} m + \\
& + \{ 7.7 \times 10^{-8} \text{ A/side} + 2.73 \times 10^{-7} \text{ A/side} \} m = \\
& = \{ 3.456 \times 10^{-8} \text{ A/side} \} (166 \text{ sides}) = \\
& = 5.74 \times 10^{-4} \text{ A},
\end{aligned}$$

and therefore the total photocurrent:

$$\begin{aligned}
I_L &= I_L(A1) + I_L(A2) = 7.81 \times 10^{-4} \text{ A} + 5.74 \times 10^{-4} \text{ A} = \\
&= 1.355 \times 10^{-3} \text{ A}.
\end{aligned}$$

Substituting our values in Eq.(18) with $A = 1.97 \text{ cm}^2$ we get for the saturation current:

$$I_s = 5.0 \times 10^{-8} \text{ A}$$

Then from Eq. (19) we get the I-V characteristic for this configuration which is shown in figure (24).

At, $\lambda = 0.5 \text{ } \mu\text{m}$, we get:

$$I_{d1}(A1) = 6.14 \times 10^{-8} \text{ A/side},$$

$$I_{b1}(A1) = 4.77 \times 10^{-7} \text{ A/side},$$

$$I_{d2}(A1) = 1.54 \times 10^{-8} \text{ A/side},$$

$$I_{b2}(A1) = 1.31 \times 10^{-7} \text{ A/side},$$

$$I_{d3}(A1) = 7.87 \times 10^{-7} \text{ A/side},$$

$$I_{b3}(A1) = 5.88 \times 10^{-8} \text{ A/side},$$

$$I_{d1}(A2) = 3.0 \times 10^{-8} \text{ A/side},$$

$$I_{b1}(A2) = 2.24 \times 10^{-7} \text{ A/side},$$

$$I_{d2}(A2) = 3.96 \times 10^{-8} \text{ A/side},$$

$$I_{b2}(A2) = 3.36 \times 10^{-7} \text{ A/side},$$

$$I_{d3}(A2) = 8.50 \times 10^{-7} \text{ A/side,}$$

$$I_{b3}(A2) = 6.63 \times 10^{-8} \text{ A/side,}$$

and finally:

$$\begin{aligned} I_L &= I_L(A1) + I_L(A2) = 1.52 \times 10^{-3} + 1.40 \times 10^{-3} = \\ &= 2.92 \times 10^{-3} \text{ A.} \end{aligned}$$

The I-V characteristic is shown in Fig. (25).

As we see a significant improvement over the V-shaped (symmetric) surface has been achieved primarily due to optical improvement, by increasing the number of reflections.

(f) Asymmetric M-shaped Surface Cells

In the same way the M-shaped surface was created over the V-shaped cell we can also have the asymmetric M-shaped surface over the asymmetric V-shaped surface, which is shown in figure (23).

Calculations done here for this type of surface in the same analogy, like before, give us:

$$m = 111 \text{ sides; } A_1 = 65.3 \times 10^{-4} \text{ cm}^2; A_2 = 26.6 \times 10^{-4} \text{ cm}^2$$

$$A_3 = 32.64 \times 10^{-4} \text{ cm}^2; A_4 = 53.21 \times 10^{-4} \text{ cm}^2$$

getting a total area of: $A = 1.97 \text{ cm}^2$, and the photocurrents at $\lambda = 0.9 \mu\text{m}$, are:

$$I_L(A1) = 4.706 \times 10^{-6} \text{ A/side}$$

$$I_L(A2) = 1.98 \times 10^{-6} \text{ A/side}$$

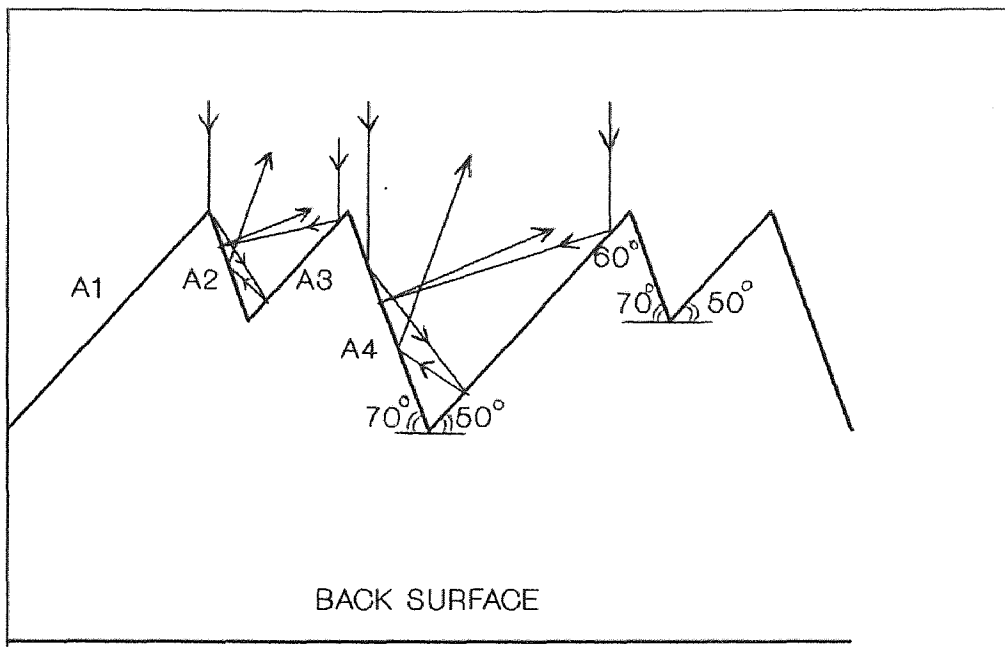


Fig.(23) An Asymmetric-M-shaped surface

$$I_L(A3) = 2.57 \times 10^{-6} \text{ A/side}$$

$$I_L(A4) = 3.456 \times 10^{-6} \text{ A/side}$$

with the total photocurrent:

$$I_L = (1.27 \times 10^{-5} \text{ A/side})(111 \text{ sides}) = 1.4 \times 10^{-3} \text{ A}$$

with: $I_s = 5.0 \times 10^{-6} \text{ A}$,

we get the I-V characteristic given in figure (24).

At $\lambda = 0.5 \mu\text{m}$, we get:

$$I_L(A1) = 9.13 \times 10^{-6} \text{ A/side,}$$

$$I_L(A2) = 4.87 \times 10^{-6} \text{ A/side,}$$

$$I_L(A3) = 5.53 \times 10^{-6} \text{ A/side.}$$

$$I_L(A4) = 8.44 \times 10^{-6} \text{ A/side,}$$

and the total photocurrent:

$$I_L = (2.8 \times 10^{-5} \text{ A/side})(111 \text{ sides}) = 3.1 \times 10^{-3} \text{ A.}$$

The I-V characteristic is shown in Fig.(25).

As in the M-shaped surface cell, the little improvement that we get over the asymmetric V-shaped cell is primarily due to some electrical and not really to optical advancement.

2.5 Noise Corrections

So far we have assumed for all configurations that the whole surface can contribute to the gain due to the

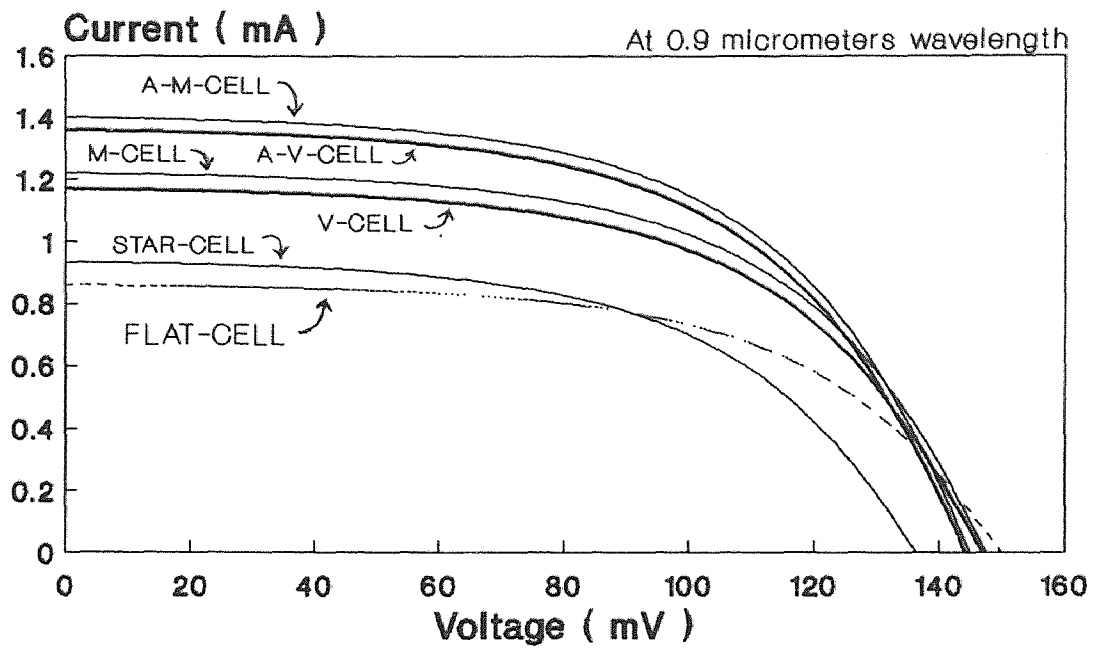


Fig.(24) I-V characteristics of the different surface configurations, for solar cells.

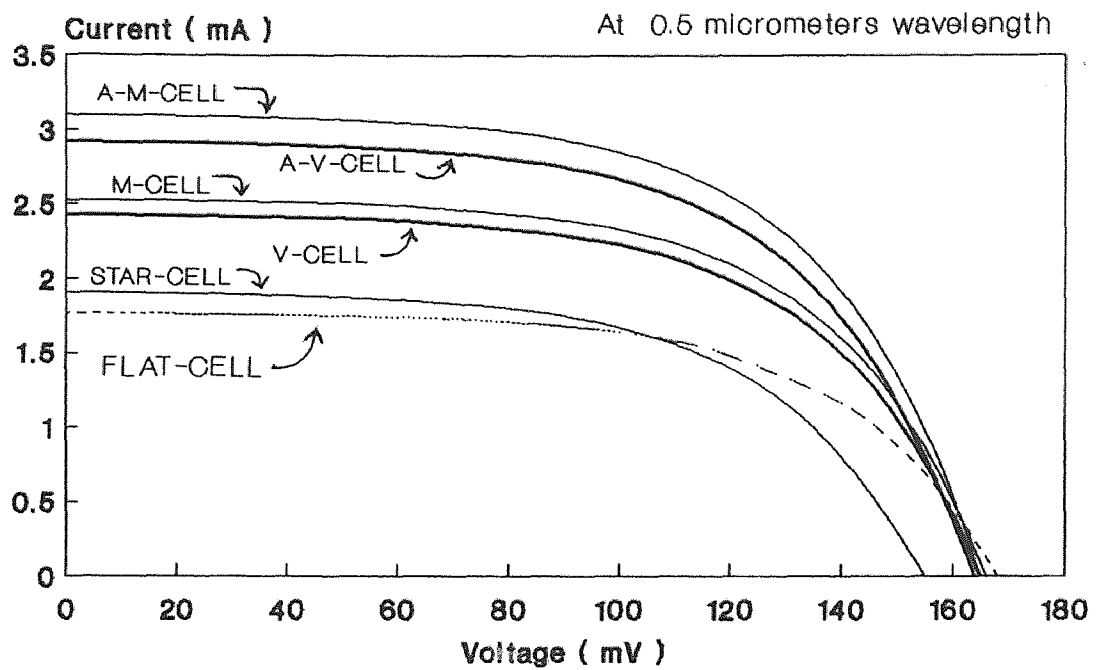


Fig.(25) I-V characteristic of the different surface configurations, for solar cells.

photogenerated current. Are we really able to make on a surface by etching or other fabrication techniques these sharp edges that we have assumed in our calculations? The answer is no. Therefore, we must make a correction to those points and see by how much this affects our I-V curves and further the behaviour of such a device.

We demonstrate this point for a V-shaped surface cell.

If we assumed, at this point, that the V-shaped surface follows the periodic triangular wave, the Fourier expansion of this configuration is given by [21]:

$$f(x) = (\Psi/2) - (4\Psi/\pi^2) \sum_{n=1,3,\dots} (1/n^2) \cos(n\pi x/h) \quad (33)$$

where Ψ is the amplitude of pattern.

Let us assume that the edges of our etched figure are rounded due to an incomplete etching process. For simplicity we may assume a flat surface which deteriorate the reflection process. A flat edge is serving as an upper bound to our noise estimation.

Substituting our amplitude, which is $\Psi = 50 \mu\text{m}$, the length $h = \Psi/\tan(\theta)$, and assuming only the first harmonic in the expansion (33), we get:

$$\text{at: } x = h, \quad f(x) = 45 \mu\text{m}$$

$$\text{at: } x = 2h, \quad f(x) = 5 \mu\text{m}$$

$f(x)$ is the lost of reflection area to further reflections more than one. The section area lost is: $\Delta S = 6.53 \times 10^{-4} \text{cm}^2$ and the flat section area: $\Delta x = 4.2 \times 10^{-4} \text{cm}^2$, as shown in Fig.(26). The new total surface area is: $A' = 1.443 \text{cm}^2 < A$ with (A) being the area as found for the V-shaped surface. Following the same procedure and calculations as done previously we can find that the new photocurrent generated at $\lambda = 0.9 \mu\text{m}$, is given by:

$$\begin{aligned} I_{d1} &= \left[\sum_j^N (J_{d1} \Delta A_j)(\xi_j) \right] m + (\Delta I_{d1}) m = \\ &= (6.57 \times 10^{-7} \text{ A/side}) (238 \text{ sides}) = \\ &= 1.56 \times 10^{-4} \text{ A} \end{aligned}$$

$$\begin{aligned} I_{b1} &= \left[\sum_j^N (J_{b1} \Delta A_j)(\xi_j) \right] m + (\Delta I_{b1}) m = \\ &= (2.38 \times 10^{-6} \text{ A/side}) (238 \text{ sides}) = \\ &= 5.66 \times 10^{-4} \text{ A}, \end{aligned}$$

where: ΔI_{d1} , ΔI_{b1} -- are the currents due to perpendicular incidence over the $(\Delta x/2)$ region on top and bottom of the flatten areas.

$$\begin{aligned} I_{d2} &= \left[\sum_j^{N'} (J_{d2} \Delta A_j)(\xi_j) \right] m + (\Delta I_{d2} + \Delta I_{d3}) m = \\ &= (2.555 \times 10^{-7} \text{ A/side})(238 \text{ sides}) = 6.08 \times 10^{-5} \text{ A} \end{aligned}$$

$$I_{b2} = \left[\sum_j^N (J_{b2} \Delta A_j)(\xi_j) \right] m + (\Delta I_{b2} + \Delta I_{b3}) m =$$

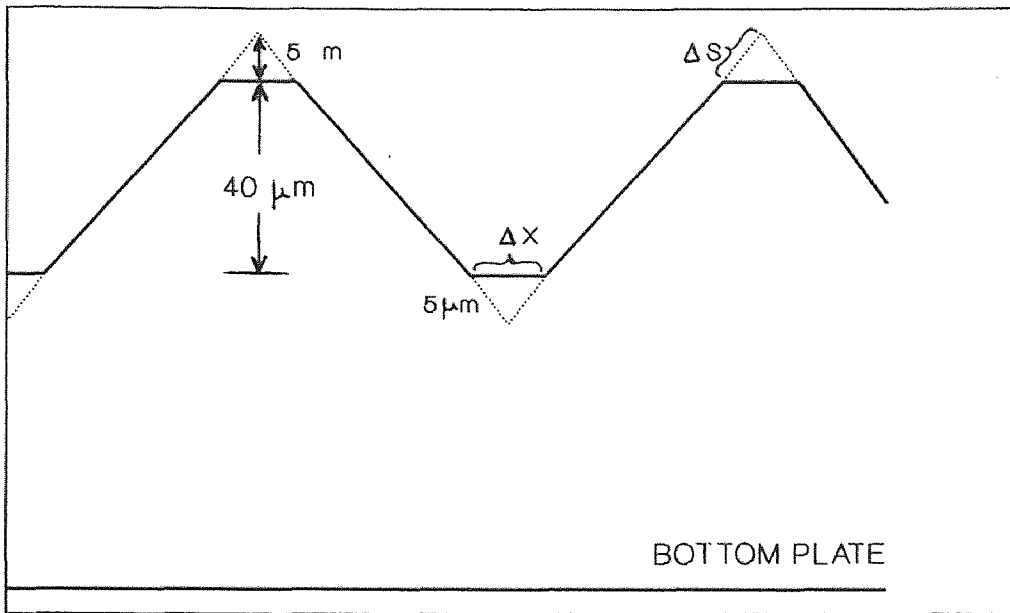


Fig.(26) The V-shaped surface after Noise Correction.

$$\begin{aligned}
&= (9.35 \times 10^{-7} \text{ A/side}) (238 \text{ sides}) = \\
&= 2.22 \times 10^{-4} \text{ A}
\end{aligned}$$

where: ΔI_{d2} , ΔI_{d3} , ΔI_{b2} , ΔI_{b3} -- are the currents due to 2nd reflection over the Δx bottom flatten region and due to 3rd reflection over a region on the adjacent side.

Therefore, the total photocurrent, at $0.9 \mu\text{m}$, is given by:

$$\begin{aligned}
I_L &= I_{d1} + I_{b1} + I_{d2} + I_{b2} = \\
&= 1.56 \times 10^{-4} + 5.66 \times 10^{-4} + 6.08 \times 10^{-5} + \\
&\quad + 2.22 \times 10^{-4} = 1.01 \times 10^{-3} \text{ A}.
\end{aligned}$$

From Eq.(18) with the area being $A' = 1.443 \text{ cm}^2$ we get the the saturation current to be: $I_s = 3.68 \times 10^{-6} \text{ A}$.

Using Eq.(19) we can find the I-V characteristic which is shown in Fig.(27), along with the flat surface cell and the V-shaped cell without the noise correction.

At $\lambda = 0.5 \mu\text{m}$, we get:

$$\begin{aligned}
I_{d1} &= (5.6 \times 10^{-8} \text{ A/side})(238 \text{ sides}) = \\
&= 1.33 \times 10^{-3} \text{ A}
\end{aligned}$$

$$\begin{aligned}
I_{b1} &= (4.42 \times 10^{-7} \text{ A/side})(238 \text{ sides}) = \\
&= 1.05 \times 10^{-4} \text{ A}
\end{aligned}$$

$$\begin{aligned}
I_{d2} &= (2.71 \times 10^{-6} \text{ A/side})(238 \text{ sides}) = \\
&= 6.46 \times 10^{-4} \text{ A}
\end{aligned}$$

$$I_{b2} = (2.08 \times 10^{-7} \text{ A/side})(238 \text{ sides}) =$$

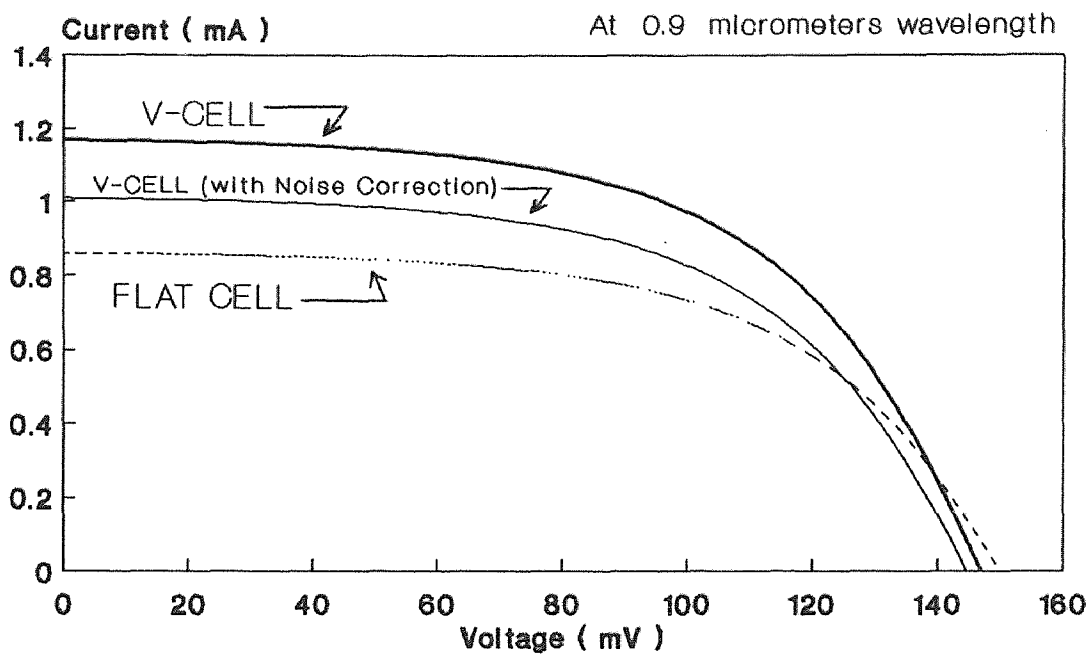


Fig.(27) I-V characteristic compared to the Noise correction for a V-cell.

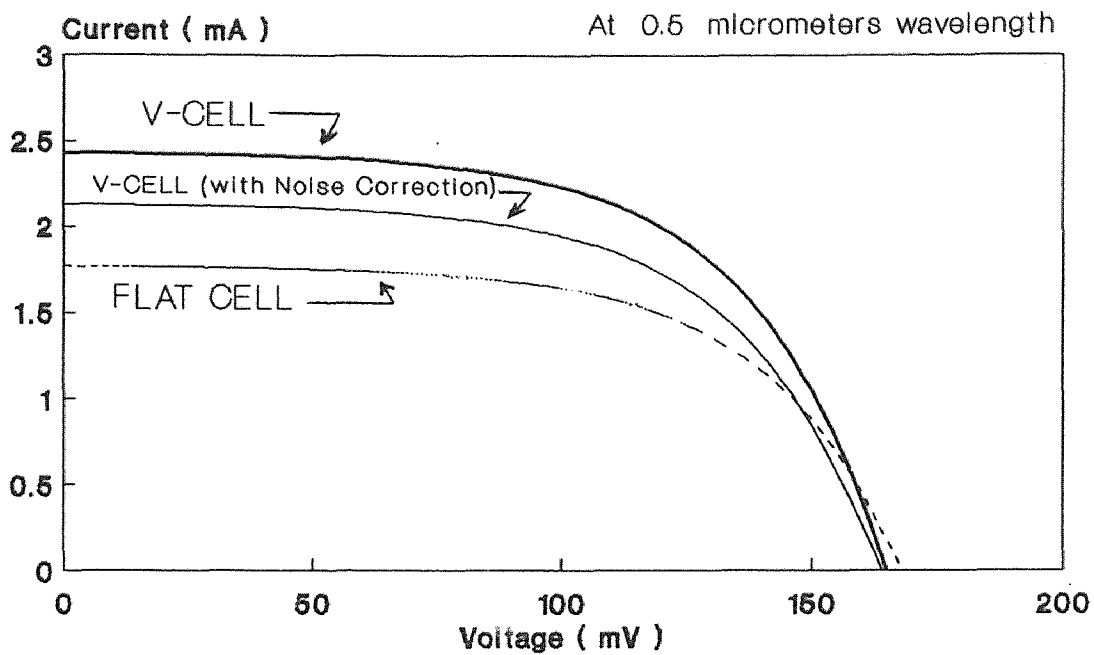


Fig.(28) I-V characteristic compared to the Noise correction for a V-cell.

$$= 4.96 \times 10^{-5} \text{ A}$$

and finally the total photocurrent is:

$$I_L = 2.13 \times 10^{-3} \text{ A}$$

The I-V characteristic is shown in Fig.(28).

It is worth noting, that, as we decrease the amplitude Ψ by keeping the total surface area constant, the noise factor will increase and, therefore, will further lower the short circuit current, making it now look comparable to the flat surface cell.

III DISCUSSION

We have shown in this work that patterned surfaces show significant improvement in the short circuit current over a flat surface solar cell of the same characteristics, while the open circuit voltage remains practically unchanged (actually reduces by only a few mV). This improvement in (I_{sc}) reaches the 62 % over the flat cell. If we account for the noise as introduced above, then the improvement in I_{sc} is only 30 %. Comparison between light illumination at $0.5 \mu\text{m}$ show an improvement in the short-circuit current I_{sc} , over the $0.9 \mu\text{m}$ wavelength. The short-circuit current almost doubled for $\lambda=0.5 \mu\text{m}$. The open circuit voltage, V_{oc} , also increased by about 12.5 %. This is due to the fact that at $\lambda=0.5 \mu\text{m}$, silicon becomes a highly absorbing material. Also most of the photogenerated current is created closer to the surface, within the depletion region and, therefore, easily collected, before recombination of carriers becomes a significant factor. It is worth pointing, that, at $\lambda=0.5 \mu\text{m}$ the energy of photons is much higher than the band-gap energy of silicon and when absorbed, some of their photonic energy will be dissipated as heat in the material, increasing lattice vibrations, and resulting in decreasing the overall cell efficiency. This heat dissipation did not affect our calculations in getting the I-V characteristics, because

it equally affected all of our configurations discussed. Any improvement in heat dissipation for flat cells will be valid for textured cells as well. Our main concern was, only to improve light collection efficiency.

Despite the improvement, of light collection efficiency shown especially for the asymmetric V-shaped and the asymmetric M-shaped surfaces, no much improvement is achieved for the open circuit voltage, V_{oc} . This is because of the subsequent increase in the saturation current as the surface area is increased.

In general, there are no reported Schottky-barrier solar cells with efficiencies of more than about 12%. It is the high saturation current I_s , (the majority-carrier thermionic current), that limits, the free flow of photo-generated current I_L . To reduce this current, I_s , a thin insulating film oxide usually is used between the metal and the semiconductor.

Experimental works done [22] show that this presence of an interfacial layer of oxide, between the metal and the semiconductor, can increase considerably the conversion efficiency of Schottky barrier solar cells without lowering the short-circuit current. This MIS device can be treated in the same manner as before with some modification for the saturation current [3]:

$$I_s = A A^{**} T^2 \exp(q\Phi_{Bn}/KT) \exp[-(q\Phi_T)^{1/2} \gamma] \quad (34)$$

where: $q\Phi_T$ -- is the average barrier height by the insulating layer,

γ -- is the insulating thickness
(usually from 10^0 A to 30^0 A)

and, A^{**} -- is the effective Richardson constant.

By solving, Eq. (19) for the V_{oc} , we get:

$$V_{oc} = (\eta KT/q) [\ln(I_L/AA^{**} T^2) + q\Phi_B/KT + (q\Phi_T)^{1/2} \gamma] \quad (35)$$

As γ increases, the V_{oc} increases but on the other hand the short circuit decreases. Therefore, for best performance one has to find an "optimum" thickness that will fit best to the above device, giving the maximum efficiency. In our case, we may have to sacrifice some of this gain in the short-circuit current due to surface multireflections in order to increase V_{oc} , for an overall adaptability.

It has been shown that, in textured solar cells the electric field lines are curved as they get closer to the surface. Therefore, the thickness of the cell can be reduced, as it has been indicated by all works done in that area [6], [8]. This may add to the compactness of these cells in small-volume environments.

IV CONCLUSION

Improvement of 30 % in light collection was shown for non-flat solar cells over flat cells. Different configurations have been analyzed, of which, the fractal like, asymmetric M-shaped cell was found the best, since it maximizes the number of light reflections without deteriorating the electrical properties of the cell. Noise in a form of non-ideal rounded patterns was analyzed too, using truncated Fourier expansion. Though much of the research nowadays is devoted to cell's materials rather than cell design, this work suggests an easy to fabricate, potentially cheap improvement of existing solar cells.

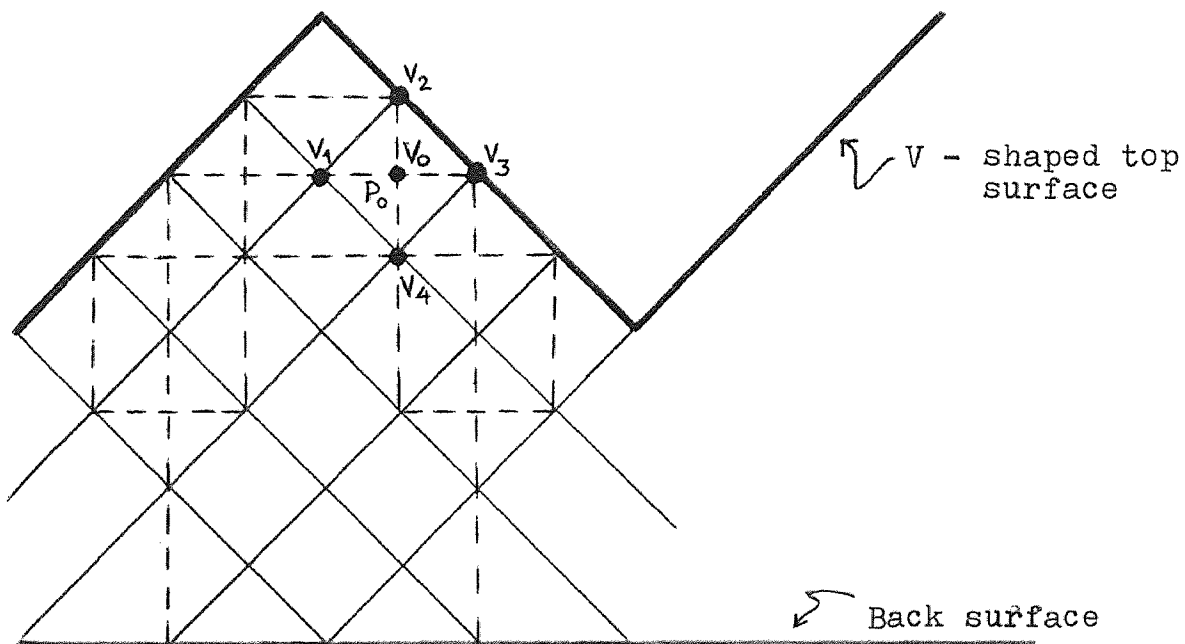
Appendix A

Numerical Solution Method:

This program uses the average-value property of Laplace's equation which states that the potential at each point is an average of its surrounding points. For that purpose we divided the space between the electrodes into squares. The potential at the center of the square is the average of the potentials of the square corners, thus:

$$V_o = 1/4 (V_1 + V_2 + V_3 + V_4)$$

where this is the result of evaluating Laplace's equation (as a function of two variables, x and y) at a point P_o in a potential field, as shown in the following figure.



EQUIPOTENTIAL LINES: Computer Programs

PROGRAM [1]

```
C   THIS PROGRAM FINDS THE EQUIPOTENTIAL LINES FOR A
C   \/-SHAPED FRONT SURFACE OF A SOLAR CELL,HAVING A
C   FLAT BACK SURFACE.-----
C   -----
C   IT DIVIDES THE AREA IN (9X9) EQUAL SQUARES AND
C   FINDS THE POTENTIAL AT THEIR CORNERS BY USING
C   THE NUMERICAL METHOD.
C   ASSUMED ALSO HERE IS THAT THE FRONT SURFACE IS
C   AT A 100 mV POTENTIAL WHILE THE BOTTOM SURFACE
C   IS AT 0 mV.-----
      COMMON P(9,9)
      DIMENSION P2(9,9)
      DO 10 J=6,9
      P(1,J)=0.0
10     P(9,J)=0.0
      DO 20 I=1,9
      P(I,1)=0.0
20     DO 21 I=2,4
      P(I,9)=0.0
21     DO 22 I=6,8
      P(I,9)=0.0
22     P(1,5)=100.0
      P(9,5)=100.0
      P(2,6)=100.0
      P(8,6)=100.0
      P(3,7)=100.0
      P(7,7)=100.0
      P(4,8)=100.0
      P(6,8)=100.0
      P(5,9)=100.0
      P(2,7)=0.0
      P(8,7)=0.0
      P(2,8)=0.0
      P(8,8)=0.0
      P(3,8)=0.0
      P(7,8)=0.0
C   NOW AT THIS POINT WE HAVE ASSIGNED ALL INITIAL
C   POTENTIAL VALUES TO THE TOP AND BOTTOM PLATES.
C   WHAT FOLLOWS THEN IS THE CALCULATIONS TO FIND
C   THE VALUES BETWEEN THE TWO PLATES BY USING A
C   FUNCTION & AN ARRAY FORMAT.-----
```

```

P(5,5)=AVERAG(5,5,0,4)
P(3,3)=AVERAG(3,3,1,2)
P(7,3)=P(3,3)
P(5,7)=AVERAG(5,7,0,2)
P(5,3)=AVERAG(5,3,0,2)
P(3,5)=AVERAG(3,5,0,2)
P(7,5)=P(3,5)
P(5,8)=AVERAG(5,8,0,1)
P(4,6)=AVERAG(4,6,-1,1)
P(6,6)=P(4,6)
P(4,4)=AVERAG(4,4,-1,1)
P(6,4)=P(4,4)
P(4,2)=AVERAG(4,2,-1,1)
P(6,2)=P(4,2)
P(4,7)=AVERAG(4,7,0,1)
P(6,7)=P(4,7)
P(5,6)=AVERAG(5,6,0,1)
P(3,6)=AVERAG(3,6,0,1)
P(7,6)=P(3,6)
P(4,5)=AVERAG(4,5,0,1)
P(6,5)=P(4,5)
P(5,4)=AVERAG(5,4,0,1)
P(5,2)=AVERAG(5,2,0,1)
P(4,3)=AVERAG(4,3,0,1)
P(6,3)=P(4,3)
P(3,4)=(4*P(4,4)-P(4,5)-P(5,4)-P(4,3))
P(7,4)=P(3,4)
P(3,2)=(4*P(4,2)-P(4,3)-P(5,2)-P(4,1))
P(7,2)=P(3,2)
P(2,4)=(4*P(3,4)-P(3,5)-P(4,4)-P(3,3))
P(8,4)=P(2,4)
P(2,5)=AVERAG(2,5,0,1)
P(8,5)=P(2,5)
P(2,2)=(4*P(3,2)-P(3,3)-P(4,2)-P(3,1))
P(8,2)=P(2,2)
P(2,3)=(4*P(3,3)-P(3,4)-P(4,3)-P(3,2))
P(8,3)=P(2,3)
P(1,4)=(4*P(2,4)-P(2,5)-P(3,4)-P(2,3))
P(9,4)=P(1,4)
P(1,3)=(4*P(2,3)-P(2,4)-P(3,3)-P(2,2))
P(9,3)=P(1,3)
P(1,2)=(4*P(2,2)-P(2,3)-P(3,2)-P(2,1))
P(9,2)=P(1,2)
J=10
DO 100 K=1,9
J=J-1
WRITE (6,90)(P(I,J),I=1,9)

```

100

```
90      FORMAT (1X,9(2X,F5.1)/)
        STOP
        END
        FUNCTION AVERAG(I,J,ICASE,ISPACE)
        COMMON P(9,9)
        AVERAG=0.25*(P(I-ISPACE,J-ICASE*ISPACE)+
+                P(I-ISPACE*ICASE,J+ISPACE)+
+                P(I+ISPACE,J+ISPACE*ICASE)+
+                P(I+ISPACE*ICASE,J-ISPACE))
        RETURN
        END
```

PROGRAM [2]

```

C   THIS PROGRAM FINDS THE EQUIPOTENTIAL LINES FOR A
C   STAR (KOCH-SNOWFLAKE CURVE)-SHAPED FRONT SURFACE
C   OF A SOLAR CELL, HAVING A FLAT BACK SURFACE.----
C   IT DIVIDES THE AREA IN (9x9) EQUAL SQUARES AND
C   FINDS THE POTENTIAL AT THEIR CORNERS BY USING
C   THE NUMERICAL METHOD.-----
C   ASSUMED IS HERE THAT THE FRONT SURFACE IS AT
C   A 100 mV POTENTIAL WHILE THE BOTTOM SURFACE IS
C   AT 0 mV.-----
      COMMON P(9,9)
      DIMENSION P2(9,9)
      DO 10 J=6,9
      P(1,J)=0.0
10     P(9,J)=0.0
      DO 20 I=1,9
20     P(I,1)=0.0
      DO 21 I=2,4
21     P(I,9)=0.0
      DO 22 I=6,8
22     P(1,9)=0.0
          P(1,5)=100.0
          P(2,6)=100.0
          P(2,7)=100.0
          P(2,8)=100.0
          P(3,8)=100.0
          P(4,8)=100.0
          P(5,9)=100.0
          P(6,8)=100.0
          P(7,8)=100.0
          P(8,8)=100.0
          P(8,7)=100.0
          P(8,6)=100.0
          P(9,5)=100.0
C   NOW WE HAVE ASSIGNED ALL INITIAL POTENTIAL
C   VALUES TO THE TOP & BOTTOM PLATES. WHAT
C   FOLLOWS NEXT IS THE CALCULATIONS TO FIND THE
C   VALUES BETWEEN THE TWO PLATES USING A FUNCTION
C   & AN ARRAY FORMAT.-----
      P(5,5)=AVERAG(5,5,0,4)
      P(3,3)=AVERAG(3,3,1,2)
      P(7,3)=P(3,3)
      P(5,3)=AVERAG(5,3,0,2)
      P(5,4)=AVERAG(5,4,-1,3)
      P(5,6)=AVERAG(5,6,0,3)
      P(4,2)=AVERAG(4,2,-1,1)
      P(6,2)=P(4,2)
      P(4,4)=(2*P(5,3)-P(4,2))
      P(6,4)=P(4,4)

```

```

P(4,6)=(2*P(5,5)-P(4,4))
P(6,6)=P(4,6)
P(3,7)=AVERAG(3,7,-1,1)
P(7,7)=P(3,7)
P(5,7)=AVERAG(5,7,-1,1)
P(5,8)=AVERAG(5,8,0,1)
P(4,7)=AVERAG(4,7,0,1)
P(6,7)=P(4,7)
P(3,5)=(4*P(5,5)-P(5,7)-P(5,3))/2
P(7,5)=P(3,5)
P(3,6)=AVERAG(3,6,0,1)
P(7,6)=P(3,6)
P(4,5)=AVERAG(4,5,0,1)
P(6,5)=P(4,5)
P(4,3)=AVERAG(4,3,0,1)
P(6,3)=P(4,3)
P(5,2)=AVERAG(5,2,0,1)
P(3,4)=(4*P(4,4)-P(4,5)-P(5,4)-P(4,3))
P(7,4)=P(3,4)
P(2,4)=(4*P(3,5)-P(2,6)-P(4,6)-P(4,4))
P(8,4)=P(2,4)
P(2,5)=AVERAG(2,5,0,1)
P(8,5)=P(2,5)
P(3,2)=(4*P(4,3)-P(3,4)-P(5,4)-P(5,2))
P(7,2)=P(3,2)
P(2,3)=(4*P(4,3)-P(4,5)-P(6,3))
P(8,3)=P(2,3)
P(2,2)=(4*P(3,2)-P(3,3)-P(4,2))
P(8,2)=P(2,2)
P(1,2)=(4*P(2,2)-P(2,3)-P(3,2))
P(9,2)=P(1,2)
P(1,3)=(4*P(2,2)-P(3,3))
P(9,3)=P(1,3)
P(1,4)=(2*P(2,4)+P(1,5)+P(1,3))/4
P(9,4)=P(1,4)
J=10
DO 100 K=1,9
J=J-1
100 WRITE (6,90)(P(I,J),I=1,9)
90  FORMAT (1X,9(1X,F5.1)/)
STOP
END
FUNCTION AVERAG(I,J,ICASE,ISPACE)
COMMON P(9,9)
AVERAG=0.25*(P(I-ISPACE,J-ICASE*ISPACE)+
+          P(I-ISPACE*ICASE,J+ISPACE)+
+          P(I+ISPACE,J+ISPACE*ICASE)+
+          P(I+ISPACE*ICASE,J-ISPACE))
RETURN
END

```


PROGRAM [3]

```

C      THIS PROGRAM FINDS THE EQUIPOTENTIAL LINES FOR AN
C      INVERTED-STAR-SHAPED FRONT SURFACE OF A SOLAR CELL
C      HAVING A FLAT BACK SURFACE.-----
C      IT DIVIDES THE AREA IN (7X7) EQUAL SQUARES AND
C      FINDS THE POTENTIAL BY USING THE NUMERICAL METHOD.
C      ASSUMED HERE IS THAT THE FRONT SURFACE HAS A
C      POTENTIAL OF 100 mV & THE BOTTOM SURFACE OF 0 mV.
      COMMON P(7,7)
      DIMENSION P2(7,7)
      DO 10 J=5,7
      P(1,J)=0.0
10     P(7,J)=0.0
      DO 20 J=1,7
20     P(I,1)=0.0
      DO 21 I=2,3
21     P(I,7)=0.0
      DO 22 I=5,6
22     P(I,7)=0.0
      P(2,6)=0.0
      P(6,6)=0.0
      P(1,4)=100.0
      P(2,5)=100.0
      P(3,5)=100.0
      P(3,6)=100.0
      P(4,7)=100.0
      P(5,6)=100.0
      P(5,5)=100.0
      P(6,5)=100.0
      P(7,4)=100.0
C      NOW AFTER HAVING ASSIGNED ALL INITIAL POTENTIAL
C      VALUES (BOUNDARY VALUES) TO THE TOP & BOTTOM
C      PLATES WE CALCULATE NEXT THE VALUES BETWEEN THE
C      TWO PLATE SURFACES BY USING A FUNCTION & AN ARRAY
C      FORMAT.-----
      P(4,3)=AVERAG(4,3,-1,2)
      P(4,5)=AVERAG(4,5,0,2)
      P(4,6)=AVERAG(4,6,0,1)
      P(2,3)=(4*P(4,3)-P(4,5))/2
      P(6,3)=P(2,3)
      P(3,4)=AVERAG(3,4,-1,1)
      P(5,4)=P(3,4)
      P(4,4)=AVERAG(4,4,0,1)
      P(2,4)=AVERAG(2,4,0,1)
      P(6,4)=P(2,4)
      P(3,2)=AVERAG(3,2,-1,1)
      P(5,2)=P(3,2)
      P(3,3)=AVERAG(3,3,0,1)

```

```

P(5,3)=P(3,3)
P(4,2)=AVERAG(4,2,0,1)
P(2,2)=(4*P(3,2)-P(3,3)-P(4,2))
P(6,2)=P(2,2)
P(1,2)=(4*P(2,2)-P(2,3)-P(3,2))
P(7,2)=P(1,2)
P(1,3)=(4*P(2,3)-P(2,4)-P(3,3)-P(2,2))
P(7,3)=P(1,3)
J=8
DO 100 K=1,7
J=J-1
100 WRITE (6,90) (P(I,J),I=1,7)
90  FORMAT (7(4X,F5.1)//)
STOP
END
FUNCTION AVERAG(I,J,ICASE,ISPACE)
COMMON P(7,7)
AVERAG=0.25*(P(I-ISPACE,J-ICASE*ISPACE)+
+          P(I-ISPACE*ICASE,J+ISPACE)+
+          P(I+ISPACE,J+ISPACE*ICASE)+
+          P(I+ISPACE*ICASE,J-ISPACE))
RETURN
END

```

PROGRAM [4]

```

C   THIS PROGRAM FINDS THE EQUIPOTENTIAL LINES FOR A
C   M-SHAPED FRONT SURFACE OF A SOLAR CELL, HAVING A
C   FLAT BACK SURFACE.-----
C   IT DIVIDES THE AREA IN (11X7) EQUAL SQUARES AND
C   FINDS THE POTENTIAL AT THEIR CORNERS BY USING THE
C   NUMERICAL METHOD.-----
C   ASSUMED HERE IS THAT THE FRONT SURFACE HAS A
C   POTENTIAL OF 100 mV AND THE BOTTOM SURFACE OF 0 mV.
C   -----
      COMMON P(11,7)
      DIMENSION P2(11,7)
      DO 10 J=5,7
      P(1,J)=0.0
10     P(11,J)=0.0
      DO 20 I=1,11
20     P(I,1)=0.0
      DO 21 I=2,3
21     P(I,7)=0.0
      DO 22 I=5,7
22     P(I,7)=0.0
      DO 23 I=9,10
23     P(I,7)=0.0
      P(2,6)=0.0
      P(6,6)=0.0
      P(10,6)=0.0
      P(1,4)=100.0
      P(2,5)=100.0
      P(3,6)=100.0
      P(4,7)=100.0
      P(5,6)=100.0
      P(6,5)=100.0
      P(7,6)=100.0
      P(8,7)=100.0
      P(9,6)=100.0
      P(10,5)=100.0
      P(11,4)=100.0
C   NOW WE HAVE ASSIGNED ALL INITIAL POTENTIAL VALUES
C   (BOUNDARY VALUES) TO THE TOP & BOTTOM SURFACES.
C   WHAT FOLLOWS NOW IS THE NUMERICAL CALCULATIONS TO
C   FIND THE VALUES BETWEEN THE TWO PLATE SURFACES.
C   IT IS DONE POINT BY POINT CAREFULLY USING A FUNCTION
C   & AN ARRAY FORMAT.-----
      P(4,3)=AVERAG(4,3,-1,2)
      P(8,3)=P(4,3)
      P(4,5)=AVERAG(4,5,0,2)
      P(8,5)=P(4,5)

```

```

P(6,3)=AVERAG(6,3,0,2)
P(5,4)=AVERAG(5,4,-1,1)
P(7,4)=P(5,4)
P(6,4)=AVERAG(6,4,0,1)
P(5,5)=AVERAG(5,5,0,1)
P(7,5)=P(5,5)
P(4,6)=AVERAG(4,6,0,1)
P(8,6)=P(4,6)
P(5,2)=AVERAG(5,2,-1,1)
P(7,2)=P(5,2)
P(5,3)=AVERAG(5,3,0,1)
P(7,3)=P(5,3)
P(6,2)=AVERAG(6,2,0,1)
P(3,4)=(4*P(4,5)-P(3,6)-P(5,6)-P(5,4))
P(9,4)=P(3,4)
P(4,4)=AVERAG(4,4,0,1)
P(8,4)=P(4,4)
P(3,5)=AVERAG(3,5,0,1)
P(9,5)=P(3,5)
P(4,2)=(4*P(5,2)-P(5,3)-P(6,2))
P(8,2)=P(4,2)
P(2,3)=(4*P(4,3)-P(4,5)-P(6,3))
P(10,3)=P(2,3)
P(3,3)=(4*P(4,4)-P(3,5)-P(5,5)-P(5,3))
P(9,3)=P(3,3)
P(3,2)=(4*P(4,2)-P(4,3)-P(5,2))
P(9,2)=P(3,2)
P(1,2)=(4*P(2,3)-P(1,4)-P(3,4)-P(3,2))
P(11,2)=P(1,2)
P(2,4)=(4*P(3,4)-P(3,5)-P(4,4)-P(3,3))
P(10,4)=P(2,4)
P(2,2)=(4*P(3,3)-P(2,4)-P(4,4)-P(4,2))
P(10,2)=P(2,2)
P(1,3)=(4*P(3,3)-P(3,5)-P(5,3))
P(11,3)=P(1,3)
J=8
DO 100 K=1,7
J=J-1
100 WRITE (6,90) (P(I,J),I=1,11)
90  FORMAT (11(1X,F5.1)//)
STOP
END
FUNCTION AVERAG(I,J,ICASE,ISPACE)
COMMON P(11,7)
AVERAG=0.25*(P(I-ISPACE,J-ICASE*ISPACE)+
+          P(I-ISPACE*ICASE,J+ISPACE)+
+          P(I+ISPACE,J+ISPACE*ICASE)+
+          P(I+ISPACE*ICASE,J-ISPACE))
RETURN
END

```

Appendix B

Photogenerated Current:

This program calculates the inhomogeneous total photogenerated current out of a Schottky barrier solar cell. The ray tracing method used is based on the amount of light transmitted into the cell per section (of area A) due to surface reflections, as shown in Figs. 14, 15, 16, 17, 20, 23. Equations (2) and (17) for the depletion region photocurrent (J_d) and the bulk photocurrent (J_b) were used respectively in finding the total photogenerated current.

The logic of this program is the same as shown in the analysis -calculations of the surface configurations in the body (section 2.4) of this work. The summation of currents collected from each surface section is represented in this program with a series of loops (one per reflection).

Finally from the total photocurrent calculated we can get through another loop a data for the I-V characteristic.

PHOTOGENERATED CURRENT: Computer Program

```
C THIS PROGRAM CALCULATES THE PHOTOCURRENT (IT)
C AND THEN GIVES US A DATA BASED ON THE ABOVE FOR
C THE I-V CHARACTERISTIC OF A V-SHAPED SURFACE
C CELL CURVED BY 50 dg. THIS PROGRAM WAS ALSO USED
C FOR THE OTHER CONFIGURATIONS AT 50 dg SURFACE
C CURVATURE.
C EXPLANATION OF SYMBOLS:
C   THI=INCIDENT ANGLE (deg)
C   ALFA=ABSORPTION COEFFICIENT (1/cm)
C   W= DEPLETION WIDTH (cm)
C   L= CELL'S TOTAL LENGTH/DEPTH (cm)
C   N= No. OF STRIPS/PATCHES
C   Q=ELECTRON CHARGE (Cb)
C   F=No. OF PHOTONS PER (cm**2-sec-bandwidth)
C   N1,N2= INDEX OF REFRACTIONS FOR AIR & SILICON
C   LP=DIFFUSION LENGTH FOR HOLES (MINORITY) (cm)
C   EG= GAP ENERGY (J)
C   K=BOLTZMANN'S CONSTANT (1.38 x 10E-23)(J/K)
C   T=TEMPERATURE (K)
C   A11=EFF. RICHARDSON'S CONSTANT (110 A/cm-2 K-2)
C   R=REFLECTIVITY
C   T=TRANSMITTANCE
C   YI=TOTAL DEPTH INTO CELL (LINEAR&CURVED PARTS)
C   ID=PHOTOCURRENT FROM DEPLETION
C   IB=PHOTOCURRENT FROM BULK (BODY)
C   MF=MULTIPLICITY FACTOR (FOR THE FIELD)
C   IT=TOTAL PHOTOCURRENT (A)
C   FB=BARRIER HEIGHT (J)
C   IS=SATURATION CURRENT (A)
C   V= VOLTAGE (V)
C -----
C THIS PROGRAM IS DOING A LOOP FOR EACH PHOTOCURRENT
C GENERATED OUT OF EACH STRIP/PATCH AND THEN ADDS
C THEM TOGETHER TO FIND THE TOTAL. FINALLY IN
C ANOTHER SIMPLE LOOP CALCULATES THE I-V DATA.
C
C ALL VARIABLES HAVE TO BE REAL IN THE PROGRAM.
C   REAL THI,ALFA,W,L,N,Q,F,N1,N2,LP,RD,EG,K,T,A11
C   REAL DEG,THR,ALFA1,R1,W1,XI,SIDES,S,AREA,TH,RI
C   REAL TI,JDP1,IDL,DYI1,YI1,ID,IB,JBK,IBK,DI,YI
C   REAL MF,IDPL1,IB11,ID1,IB1,THI1,THR1,ALFA2,R2
C   REAL S1,T2,W2,KK,RI1,JDP2,IDL2,DYI2,YI22,JBK2
C   REAL IBK2,IDF,IBF,DI2,YI2,MF2,IDPL2,IB22,ID2
```

```

REAL IB2,IT,FB,KT,IS,VF,V,I
PRINT *, 'ENTER YOUR VALUES:THI,...,A11'
READ *,THI,ALFA,W,L,N,Q,F,N1,N2,LP,EG,K,T,A11
RD=0.0174532
C CONVERTS DEGREES TO RADIANS
DEG=57.296083
C CONVERTS RADIANS TO DEGREES
THI=THI*RD
THR=ASIN((N1/N2)*SIN(THI))
ALFA1=ALFA/COS(THR)
R1=(SIN(THI-THR)**2)/(SIN(THI+THR)**2)
W1=W/COS(THR)
XI=(L/2)/TAN(THI)
SIDES=1/XI
S=(L/2)/SIN(THI)
AREA=S*SIDES
TH=10*RD
RI=S/N
T1=1-R1
JDP1=Q*T1*F*(1-EXP(-ALFA1*W1))
IDL=JDP1*RI
DYI1=RI*TH
YI1=0.005+(RI*SIN(THI-TH))+DYI1
JBK=(Q*T1*F)*((ALFA1*LP)/(ALFA1*LP+1))*EXP(-ALFA1*W1)
IBK=JBK*RI
ID=0.0
IB=0.0
C THIS LOOP CALCULATES THE PHOTOCURRENT DUE TO FIRST REFLECTION
DO 100 DI=2,N,1
  DYI=(DI*RI)*TH
  YI=0.005+(DI*RI)*SIN(THI-TH)+DYI
  MF=YI1/YI
  IDPL1=IDL*MF
  ID=ID+IDPL1
  IB11=IBK*MF
  IB=IB+IB11
100 CONTINUE
ID1=(IDL+ID)*SIDES
PRINT *, 'ID1=',ID1, ' AMPS'
IB1=(IBK+IB)*SIDES
PRINT *, 'IB1=',IB1, ' AMPS'
THI1=3*THI-(180*RD)
IF (THI1.LT.0.0) THI1=-THI1
THR1=ASIN((N1/N2)*SIN(THI1))
ALFA2=ALFA/COS(THR1)
R2=((SIN(THI1-THR1))**2)/((SIN(THI1+THR1))**2)
S1=(S*COS(THI))/(SIN(60*RD))
T2=1-R2
W2=W/COS(THR1)
KK=N*(S1/S)
RI1=RI

```

```

JDP2=Q*T2*F*R1*(1-EXP(-ALFA2*W2))
IDL2=JDP2*RI1
DYI2=RI1*TH
YI22=0.005+(RI1*SIN(THI-TH))+DYI2
JBK2=(Q*T2*F*R1)*((ALFA2*LP)/(ALFA2*LP+1))*EXP(-ALFA2*W2)
IBK2=JBK2*RI1
IDF=0.0
IBF=0.0
C THIS LOOP CALCULATES THE PHOTOCURRENT DUE TO SECOND REFLECTION
DO 200 DI2=2, KK, 1
  DYI2=(DI2*RI1)*TH
  YI2=0.005+(DI2*RI1)*SIN(THI1-TH)+DYI2
  MF2=YI22/YI2
  IDPL2=IDL2*MF2
  IDF=IDF+IDPL2
  IB22=IBK2*MF2
  IBF=IBF+IB22
200 CONTINUE
  ID2=(IDL2+IDF)*SIDES
  PRINT *, 'ID2= ', ID2, ' AMPS'
  IB2=(IBK2+IBF)*SIDES
  PRINT *, 'IB2= ', IB2, ' AMPS'
  IT=ID1+IB1+ID2+IB2
  PRINT *, 'IT= ', IT, ' AMPS'
  FB=(0.666)*EG
  KT=K*T
  IS=AREA*A11*(T**2)*(EXP(-(FB/KT)))
  PRINT *, 'IS= ', IS, ' AMPS'
  VF=(ALOG((IS+IT)/IS))/38.65
  PRINT *, 'VF= ', VF, ' V'
C THIS LOOP IS FOR THE I-V CHARACTERISTIC
DO 300 V=0, VF, 10E-3
  I=IT+IS*(1-EXP(38.65*V))
  PRINT *, 'V= ', V, ' V ---', ' I= ', I, ' AMPS'
300 CONTINUE
END

```


B I B L I O G R A P H Y

- [1] S.M. Sze, Semiconductor Devices Physics and Technology. New York: John Wiley & Sons, Inc., 1985, pp. 8-28, 30-107, 159-171, 252-258, 287-300.
- [2] B.G. Streetman, Solid State Electronic Devices, 2nd Ed., New Jersey: Prentice-Hall, Inc., 1980, pp. 52-90, 93-193, 210-218.
- [3] S.M. Sze, Physics of Semiconductor Devices, 2nd Ed. New York: John Wiley & Sons, Inc., 1981, pp. 7-60, 245-311, 760-763, 790-838.
- [4] Y. Hamakawa, Photovoltaic Power, Scientific American, vol. 256, Apr. 1987, pp. 86-92.
- [5] M.A. Fischetti, Photovoltaic-cell Technologies Joust for Position, IEEE Spectrum, Vol. 21, no. 3, March 1984, pp. 40-47.
- [6] R.A. Arndt, J.F. Allison, J.G. Haynos, and A. Meulenbergh, Jr., Optical Properties of the COMSAT Non-Reflective Cell, The 11th IEEE Photovoltaic Specialists Conference, May 1975, pp. 40-43.
- [7] A. Meulenbergh, Jr., J.F. Allison, R.A. Arndt, and J.G. Haynos, Radiation Damage to the COMSAT Non-Reflective Cell, The 11th IEEE Photovoltaic Specialists Conference, May 1975, pp. 204-208.
- [8] C.R. Baraona and H.W. Brandhorst, V-Grooved Silicon Cells, The 11th IEEE Photovoltaic Specialists Conference, May 1975, pp. 44-48.
- [9] P. Campbell and M.A. Green, Light Trapping Properties of Pyramidally Textured Surfaces, Journal of Applied Physics, Vol. 62, July 1987, pp. 243-249.
- [10] T.I. Chappell, The V-Grooved Multijunction Solar Cell, IEEE Transactions on Electron Devices, Vol. ED-26, No. 7, July 1979, pp. 1091-1097.
- [11] W.T. Matzen, S.Y. Chiang, and B.G. Carbajal, A Device Model for the Tandem Junction Solar Cell, IEEE Transactions on Electronic Devices, Vol. ED-26, No. 9, September 1979, pp. 1365-1368.
- [12] J. Wollard and G. Zorpette, Technology '89: Power and Energy, IEEE Spectrum, Vol. 26, No. 1, January 1989, pp. 56-58.

- [13] R.F. McOuat and D.L. Pulfrey, Analysis of Silicon Schottky Barrier Solar Cells, The 11th IEEE Photovoltaic Specialists Conference, May 1975, pp. 371-375.
- [14] D.L. Pulfrey, Photovoltaic Power Generation, Van Nostrand Co., 1978, pp. 20, 72-76, 85-91, 100-113.
- [15] E.S. Young, Fundamentals of Semiconductor Devices. New York: McGraw-Hill Book Co., 1978, pp. 32-51, 147-169.
- [16] D.L. Pulfrey and R.F. McOuat, Schottky-barrier Solar Cell Calculations, Applied Physics Letters, Vol.24, No.4, February 1974, pp. 167-169.
- [17] F. Abeles, Optical Properties of Solids. Amsterdam: North-Holland Publishing Co., 1972, pp. 93-119.
- [18] E.D. Palik, Handbook of Optical Constants of Solids. New York: Academic Press, Inc., 1985, pp. 286-295, 547-569.
- [19] J.R. Meyer - Arendt, Introduction to Classical and Modern Optics. New Jersey: Prentice-Hall, Inc., 1984, pp. 298-307.
- [20] J.D. Kraus, Electromagnetics. New York: McGraw-Hill Book Co., 1984, pp. 287-294.
- [21] Handbook of Mathematical Formulas, Tables, Graphs, Functions, Transforms, M.Fogiel and Staff of Research and Education Association. New York: Research and Education Association, 1980, pp. 652-659.
- [22] R. Singh and J. Shewchum, Current Conduction in Schottky Barrier Solar Cells with an Interfacial Layer, Photovoltaics and Materials Conference, Vol.6, Winnipeg: August 15-20, 1976, pp. 147-149.
- [23] R.F. McOuat and D.L. Pulfrey, A Model for Schottky-barrier Solar Cell Analysis, Journal of Applied Physics, Vol.47, No.5, May 1976, pp. 2113-2119.
- [24] P. Rappaport, The Photovoltaic Effect and its Utilization, RCA Review, Vol.20, Sept. 1959, pp. 373-397.
- [25] C.E. Backus, Solar Cells. New York: IEEE Press, Inc., 1976, pp.1-13, 171-191, 306-311.

- [26] R.J. Stirn and Y.-C.M. Yeh, The AMOS Cell an Improved Metal-Semiconductor solar Cell, The 11th IEEE Photovoltaics Specialists Conference, May 1975, pp.437-438.
- [27] Y.-C.M. Yeh and R.J. Stirn, Improved Schottky Barrier Solar Cells, The 11th IEEE Photovoltaics Specialists Conference, May 1975, pp. 391-397.
- [28] A.M. Cowley and S.M. Sze, Surface States and Barrier-Height of Metal-Semiconductor Systems, Journal of Applied Physics, Vol. 36, No.10, October 1965, pp.3212-3220.
- [29] H.C. Card, E.S. Yang, and P. Panayotatos, Peaked Schottky-barrier Solar Cells by Al-Si Metallurgical Reactions, Applied Physics Letters, Vol.30, No.12, June 1977, pp. 643-645.
- [30] W.A. Anderson and R.A. Milano, I-V Characteristics for Silicon Schottky Solar Cells, Proceedings of the IEEE, January 1975, pp.206-208.
- [31] O.M. Nielsen, On the Surface Recombination Current of Metal-insulator Semiconductor Inversion Layer Solar Cells, Journal of Applied Physics, Vol.52, No.9, September 1981, pp.5870-5872.
- [32] W.W. Lloyd, Fabrication of an Improved Vertical Multijunction Solar Cell, The 11th IEEE Photovoltaics Specialists Conference, May 1975, pp. 349-355.
- [33] D. Redfield, Enhanced Photovoltaic Performance of Thin Silicon Films by Multiple Light Passes, The 11th IEEE Photovoltaic Specialists Conference, May 1975, pp.431-432.
- [34] P. Campbell and M.A. Green, The Limiting Efficiency of Silicon Solar Cells under Concentrated Sunlight, IEEE Transactions on Electron Devices, Vol. ED-33, No.2, February 1986, pp. 234-239.
- [35] C.H. Henry, Limiting Efficiencies of Ideal Single and Multiple Energy Gap Terrestrial Solar Cells, Journal of Applied Physics, Vol.51, No.8, August 1980.
- [36] G. Grotty, T. Daud, and R. Kachare, Front Surface Passivation of Silicon Solar Cells with Antireflection Coating, Journal of Applied Physics, Vol.61, No.8, April 1987.

- [37] D. Redfield, Multiple-pass Thin-film Silicon Solar Cell, Applied Physics Letters, Vol.25, No.11, December 1974, pp. 647-648.
- [38] E. Yablonovitch and G.D. Cody, Intensity Enhancement in Textured Optical Sheets for Solar Cells, IEEE Transactions on Electron Devices, Vol. ED-29, No.2, February 1982, pp. 300-305.
- [39] M.L. Theye, Investigation of the Optical Properties of Au by Means of Thin Semitransparent Films, Physical Review B, Vol.2, No.8, October 1970, pp.3060-78.
- [40] E. Valkonen, B. Karlsson, and C.-G. Ribbing, Solar Optical Properties of Thin Films of Cu, Ag, Au, Cr, Fe, Co, Ni, and Al, Solar Energy, Vol.32, No.2, 1984, pp.211-222.
- [41] M.V. Klein and T.E. Furtak, Optics, 2nd Ed., New York: John Wiley & Sons, Inc., 1986, pp. 71-127.
- [42] R.J. Komp, Practical Photovoltaics, Autec Publications, Inc., 1981, pp.89-107, 128-129.
- [43] M. Wolf, Outlook for Si Photovoltaic Devices for Terrestrial Solar-energy Utilization, Journal of Vacuum Science Technology, Vol.12, No.5, September/October 1975, pp.984-999.